Energy 320 (2025) 135145

Contents lists available at ScienceDirect

Energy

journal homepage: www.elsevier.com/locate/energy

# Optimizing expressway battery electric vehicle charging and mobile storage energy truck scheduling: A two-stage approach to improve photovoltaic generation utilization

Dawei Wang [a], Jingwei Guo [b,*], Yongxiang Zhang [c], Qingwei Zhong [d], Hongke Xu [a]

[a] School of Electronics and Control Engineering, Chang'an university, Xi'an, 710064, China
[b] Faculty of Business, City University of Macau, 999078, Macao Special Administrative Region of China
[c] School of Transportation and Logistics, National United Engineering Laboratory of Integrated and Intelligent Transportation, National Engineering Laboratory of Integrated Transportation Big Data Application Technology, Southwest Jiaotong University, Chengdu, 610031, China
[d] College of Air Traffic Management, Civil Aviation Flight University of China, Guanghan, 618307, China

ARTICLE INFO

*Keywords:*
Battery electric vehicle charging
Two-stage optimization
Column-and-constraint generation algorithm
Mobile energy storage truck scheduling
Spatial–temporal network model

ABSTRACT

Promoting the utilization of photovoltaic generation along expressways is crucial for advancing green transportation. The long-distance distribution of photovoltaic devices on expressways results in underutilized photovoltaic generation. An effective solution to this issue is to direct the charging of battery electric vehicles in an orderly manner. Nowadays, research on charging battery electric vehicles using mobile energy storage trucks has emerged as a significant area of interest. Therefore, this paper proposes a two-stage approach for optimizing the coupled relationship between battery electric vehicle charging and mobile energy storage truck scheduling along expressways for efficient photovoltaic generation resource allocation. The proposed model employs spatial–temporal network concepts for battery electric vehicles and mobile energy storage trucks to depict the interplay between transportation and energy. In the first stage, a two-layer optimization model is developed to determine the charging plans of battery electric vehicles, balancing the profits of expressway managers with the expenses incurred by battery electric vehicle drivers. The upper-layer model focuses on maximizing the net earnings of the expressway manager, whereas the lower-layer model aims to minimize the charging and parking costs for battery electric vehicle drivers. The two-layer optimization model is solved with a column-and-constraint generation algorithm. The second stage optimizes the discharge/charge power and paths for mobile energy storage trucks to effectively distribute photovoltaic generation according to grid-supplied charging loads. The case study demonstrates that the proposed method significantly boosts photovoltaic generation utilization to 81.7% and reduces main grid purchase costs to 2122.0 RMB, fostering a mutually beneficial environment and economy for expressway managers.

## 1. Introduction

In recent years, as the global landscape shifts toward green and low-carbon transportation, the integration of photovoltaic (PV) installations along expressways has surged remarkably [1]. These solar energy systems, adept at converting sunlight into electrical power, can be strategically deployed on the undulating slopes of expressways [2] or ingeniously placed atop service area edifices [3]. Such advancements herald a transformative era in expressway energy management, offering a sustainable and economically viable alternative to traditional power sources. This not only mitigates reliance on long-distance energy transmission but also curtails fossil fuel consumption, thereby playing a crucial role in reducing carbon emissions and enhancing the economic viability of expressway transportation systems.

The increasing prevalence of battery electric vehicles (BEVs) further amplifies the urgency of this research. These vehicles, powered by rechargeable batteries, are characterized by their remarkable flexibility in charging times and locations [4], making them prime candidates for synergistic integration with renewable energy sources like PV systems. Expressways, as vital arteries of cross-regional transport [5], emerge as focal points for this integration. With the popularization of low-carbon concept, expressway managers can orchestrate BEV charging protocols, guiding vehicles to optimal charging zones at times when PV generation

* Corresponding author.
*E-mail addresses:* 2021032008@chd.edu.cn, dwei1523900@163.com (D. Wang), jwguo@cityu.edu.mo, jingwei_guo@126.com (J. Guo), yongxiangzhang@swjtu.edu.cn (Y. Zhang), qingweizhong@cafuc.edu.cn (Q. Zhong), xuhongke@chd.edu.cn (H. Xu).

https://doi.org/10.1016/j.energy.2025.135145
Received 14 November 2024; Received in revised form 14 February 2025; Accepted 18 February 2025
Available online 1 March 2025

**Acronyms**

| | |
|---|---|
| BEV | Battery electric vehicle |
| MEST | Mobile energy storage truck |
| BESD | Battery energy storage device |
| ESA | Expressway service area |
| EVCS | Electric vehicle charging station |
| ES | Expressway segment |
| SPESP | Slope PV energy supply point |

is robust [6]. This strategic alignment not only diminishes dependence on conventional power grids but also propels the broader transition toward renewable energy utilization.

A BEV, defined as a vehicle solely powered by rechargeable batte ries—such as lithium iron phosphate or ternary lithium batteries [7], offers a plethora of charging modalities, ranging from rapid to leisurely charging, tailored for diverse environments including offices, parking lots, and service areas [8]. This inherent flexibility in charging time and spatial requirements facilitates the effective harnessing of PV energy across distributed regions, enabling orderly BEV charging [9]. Through the deployment of advanced information-sharing technologies [10], expressway managers can deftly coordinate BEV charging schemes, directing vehicles to charge at strategically chosen locations where PV generation is abundant. For instance, Zhang et al. have proposed innovative methodologies to guide BEV operators toward electric vehicle charging stations (EVCSs) situated in areas rich in solar energy resources [11].

Yet, the reality remains that abundant PV generation is not uniformly attainable across all expressways or their segments. The spacing of PV facilities is often dictated by road conditions, introducing uncertainty into their deployment. Furthermore, the efficiency of PV power conversion is influenced by a myriad of factors, including local weather conditions and geographical variances [12]. These complexities, coupled with the unpredictable nature of BEV charging demand, hinder efforts to enhance the utilization of PV generation merely by leveraging the flexible characteristics of charging loads. Thus, the dual temporal–spatial disparities in PV generation and BEV charging exacerbate the challenges faced by expressway managers in improving PV generation utilization.

The implementation of PV installations along expressways necessitates meticulous attention to various factors, including module siting, layout, installed capacity, and overall power generation efficiency. Critical considerations encompass topography, sunlight exposure, and shadowing effects to ensure optimal solar radiation capture. Additionally, the layout must maximize the use of available space along building rooftops, slopes, and tunnel tops, although practical constraints often render these arrangements somewhat arbitrary. Concurrently, the positioning of stationary energy storage systems, designed to store surplus PV generation, should be executed with strategic foresight rather than random placement [13]. Inefficiencies arise in regions marked by low electricity consumption and limited solar energy utilization, resulting in a pronounced regional imbalance between PV generation supply and charging demand.

This imbalance is fundamentally linked to power scheduling, a topic extensively explored within the electricity sector. While numerous studies have investigated the application of mobile energy storage systems (MESSs) for power scheduling [14], a critical distinction exists between these studies and the specific context of BEV charging power scheduling. Primarily, MESS designs emphasize long-distance transmission and overall power supply efficacy, focusing on high-voltage transmission and distribution within the power grid. In contrast, PV installations along expressways cater specifically to the charging needs of BEVs, where DC fast-charging stations typically operate at output voltages ranging from 400 V to 750 V, and AC slow-charging stations function at 200 V to 240 V, ensuring both efficiency and safety [15]. Consequently, conventional grid technologies associated with MESSs cannot be directly applied to the power scheduling of PV generation along expressways.

Moreover, MESSs are frequently utilized as emergency backup power sources for critical facilities such as hospitals and data centers. However, various constraints—geographical, personnel-related, and otherwise—significantly impede their operational effectiveness, particularly on expressways. For instance, a sudden heavy snowfall in Hubei Province, China, in 2024, rendered roads and facilities impassable, leading to significant congestion among BEVs on expressways [16]. Under such conditions, normal operations became increasingly challenging, and MESSs are proved inadequate in maintaining BEV functionality. Lastly, transformers with limited capacity struggle to dynamically adjust charging power to meet the escalating charging demands of BEVs. Thus, traditional MESS frameworks fall short in addressing the critical imbalance between PV supply and charging demand within expressway contexts.

An effective solution is to optimize the dispatch of mobile energy storage trucks (MESTs) to provide power for BEV charging. An MEST with mobility and flexibility is a large vehicle equipped with a battery energy storage device (BESD) [17]. In contrast to the stationary energy storage systems, MESTs are able to be connected to the power infrastructure at various sites along expressways [18]. The feature enables the BESD installed in MESTs to be charged in areas with abundant PV generation before being dispatched to expressway EVCSs with high charging demands. MESTs, while capable of accommodating the charging needs of EVs on expressways, still face the following three challenges:

(1) Unlike PV and stationary energy storage systems, MESTs are flexible and can serve BEVs that require recharge regardless of time and space constraints. Mathematically and logically, there exists a spatial–temporal relationship between MESTs and BEVs. Therefore, a spatial–temporal network model is required to accurately describe the power transfer process from MESTs to BEVs, considering geographical variations in charging requirements.
(2) The practical issue for BEV drivers is the acceptability and cost of a charging scheme. Thus, how to accurately capture the driving behavior characteristics of BEVs and find the optimal economic solution that benefits BEV drivers under a set of constraints, including charging and parking cost functions, is an urgent problem.
(3) From the perspective of expressway managers, the management of MESTs involves issues such as discharging, charging power, and paths, which will have a direct impact on improving the imbalance between PV-generating supply and charging demand. Furthermore, there is a conflict between the objectives of the expressway manager and BEVs, and finding a way to balance their connection is a technical issue that needs to be taken into account.

In response to the above challenges, this paper presents a two-stage scheduling approach for efficient utilization of PV generation in BEV charging and MESTs on expressways. By improving PV generation utilization, the proposed approach supports the integration of renewable energy into transportation systems, contributing to national and regional goals for sustainability and carbon neutrality. The main contributions of this study are summarized as follows:

(1) A two-stage scheduling approach is proposed for managing the scheduling of MESTs and BEV charging on expressways. The first stage focuses on revealing the spatial and temporal imbalance between PV generation supply and BEV charging demand. In the second stage, MESTs are assigned to transport PV generation unconsumed by BEV charging under first-stage calculations to high-demand locations, thereby alleviating the supply–demand imbalance of expressway energy.

**Table 1**
Comparison of studies related to the PV generation for BEV charging.

| Reference | Focus | Main objective | Scenario | Disadvantage |
|---|---|---|---|---|
| [19] | Cooperative scheduling strategy of energy storage and BEVs in a residential building integrated PV | Improve the utilization of solar energy resources | Residential building | Driving activities for BEV not extensively discussed |
| [20] | Collaborative planning for distributed energy station and BEV charging loads | Minimize annualized total cost | City | Ignorance of battery level impacts on changing BEV charging loads |
| [21] | Optimizing the number of EVCSs in microgrid integrated with a PV plant | Maximize the system profit | University campuse | Lack of discussions on initial battery level for BEVs |
| [22] | Smart electric vehicles charging with centralized vehicle-to-grid capability | Minimize net-load variance and improve PV penetration levels | City | Lack of discussions on selecting different charging stations |
| [23] | Environmentally oriented optimal design of an EVCS with PV devices | Maximize the self-consumption of local PV generation | Single EVCS | Limited focus on BEV charging scenarios and lack of exploration into the interaction between multiple EVCSs |
| [12] | Integration of BEVs charging and PV generation in the power system | Maximize PV generation utilization | City | Limited focus on BEV charging scheduling |
| [24] | Multi-mode PV-assisted charging stations. | Maximize operational profits | City | Lack of discussions on traffic conditions |
| [25] | Optimal energy scheduling strategy for BEV charging at EVCS with a grid-connected PV system | Increase BEV charging from the PV system | Urban area | Potential challenges in adapting the model to PV generation in different regions |
| [26] | Optimal location and capacity for EVCS with PV generation that best fit the distribution of charging demands | Reduce charging costs | City | Limited focus on battery level impacts on charging demands |
| [27] | Analysis to specifically look at the synergies of PV and EV charging stations | Increase store selection and profit | – | Lack of discussions on charging demands |
| [28] | Management of charging process considering PV generation | Improve stability in power grids | – | Lack of discussions on reshaping charging loads |
| [29] | Energy trading framework for EVCSs equipped with distributed PV system | Improve EVCS operating profits | City | Ignorance of discussions on the relationship between the BEV battery level and its location |

(2) The first stage involves building a spatial–temporal network model of BEVs to characterize the connection between battery level and location, allowing for the visualization of geographic variations in charging demands. Specifically, the model is a two-layer optimization model, with the upper layer aiming to maximize revenue and the lower layer minimizing charging and parking costs. Meanwhile, the Column-and-Constraint Generation (C&CG) algorithm is utilized to resolve the conflict between upper and lower layer objectives.
(3) In the second stage, the spatial–temporal network of MESTs is introduced to construct a model that accurately describes its movement and changes in electricity storage in energy supply and demand regions, thereby simulating the transmission of electricity from MEST to BEVs. Meanwhile, a mixed integer linear programming (MILP) model is developed to optimize the scheduling of MESTs, determining the optimal discharging and charging power and paths for MESTs.
(4) The performance of the proposed two-stage model is evaluated through a case study, with four comparison cases designed to ensure the model's optimal validity. Results show that the method can generate optimal schedules for BEV charging and MESTs. This helps increase the utilization of PV generation on expressways, assisting BEV drivers in considering costs.

The remainder of this study is structured as follows. A literature review on PV generation for BEV charging and the MEST is presented in Section 2. The brief problem description is introduced in Section 3. Section 4 describes the comprehensive methodological framework of the two-stage method. This part comprises BEV charging scheduling in the first stage and MEST scheduling in the second stage. The results and discussions of the case study regarding the proposed two-stage method are detailed in Section 5. Section 6 offers a thorough overview of the findings and provides insight into the future study.

## 2. Literature review

This section reviews existing research on PV generation for BEV charging, MEST scheduling, and the key motivations driving this study.

### 2.1. Photovoltaic generation for battery electric vehicle charging

The integration of PV generation technology into the expressway system is an innovative application. Therefore, existing studies primarily concentrate on PV generation and expressway traffic organization. Despite a lack of literature on the organic combination of BEVs and PV generation on expressways, some studies from other related fields are available (see Table 1).

PV generation is a sustainable and eco-friendly energy solution for BEV charging. It converts solar energy into DC electricity, reducing reliance on traditional energy sources, lowering carbon emissions, and aiding in the fight against climate change. However, the use of PV generation for BEV charging on expressways is facing several challenges. First, scholars agree that optimizing charging management is crucial for combining PV and BEV charging. Current studies focus on layout [26], technical analysis [27], planning [20], management [28], intelligent system design [29], and strategy optimization [12] of charging stations. For example, Ullah et al. optimized BEV charging at a solar-based grid-tied charging station to improve PV power utilization [12]. In fact, these studies primarily focus on static optimization of pre-planning and

**Table 2**
Comparison of studies related to MEST scheduling.

| Reference | Focus | Main objective | Scenario | Disadvantage |
|---|---|---|---|---|
| [31] | Two-layer optimization strategy for fixed and mobile energy storage with PV | Minimize operating costs and the voltage offset | Distribution network in city | Lack of discussion on traffic models for mobile energy storage |
| [32] | Stochastic planning of resilient power distribution systems with the mobile energy storage system (MESS) against earthquakes | Minimize total investment cost and the expected loss of loads | – | Ignorance of dynamic relationship between temporal dimension and spatial dimension for the MESS |
| [33] | Stochastic energy management and scheduling of renewable microgrid with the MESS and demand response | Minimize operation costs | – | Lack of discussion on traffic conditions between microgrid nodes for MESS scheduling |
| [34] | Two-phase MESS day-ahead operation scheduling | Minimize net-load variance and improve PV penetration levels | Sub-urban area | May face challenges in scenarios of complex traffic and unbalanced spatial distribution of solar energy |
| [35] | Load restoration strategy considering fixed and mobile energy storage systems | Maximize the total restored weighted power of the loads | Power distribution systems in city | Lack of detailed discussion on temporal dimension model for the MESS |
| [36] | Distribution system with multi-microgrids and mobile energy storage in extreme operating conditions | Improve the resilience of the system | – | Limited focus on mobile energy storage scheduling |
| [37] | Collaborative optimization with both an MESS and a stationary energy storage system in distribution networks | Minimize encompassing hybrid energy storage investment costs, grid operation costs, and the load shedding penalty costs | City | Applications limited to specific traffic scene and single MESS |
| [38] | Joint framework with voltage regulators operation and routing MESSs | Minimize real power loss and MESS traveling costs | – | Potential challenges in complex traffic and energy demand contexts |

configuration of charging facilities, strategies, and resources, without monitoring and adjustment of time-space interaction.

Second, despite the fact that some researchers begin to focus on the coupled relationship between PV generation and BEV charging demand, their main emphasis is on the utilization of PV generation at each spatial location [30]. For instance, Abdalla et al. developed an energy scheduling strategy in urban areas based on the PV generation curve, BEV arrival and departure times, and the energy required for each BEV to increase PV generation consumption [25]. Notably, the study is conducted on urban roads, where BEVs are allowed to choose from EVCSs with PV installations, unlike on expressways. In addition, compared to expressways, PV generation in cities can be easily dispatched through the grid system, enabling technological advancements with existing equipment.

In summary, the expressway scenario is fundamentally different from the urban road scenario. EVCSs in expressway service areas (ESAs) primarily serve long-distance electric vehicles for charging on the way, whereas the distance between each ESA poses challenges for charging BEVs. Furthermore, PV generation in different ESAs varies depending on its location and weather conditions, and a BEV's itinerary directly influences its consumption. Therefore, modeling the battery state at each space–time point alongside BEV trips is crucial for developing effective BEV charging strategies in the expressway scenario. In addition, BEVs traveling on expressways must select routes based on their trip's starting and ending points, in contrast to urban road BEVs that can freely choose EVCSs. A high-speed and long-distance trip makes it impractical and uneconomical for a BEV to change its route or abandon it. These considerations underscore the necessity for a revised methodology.

### 2.2. Mobile energy storage truck scheduling

The management of PV generation and BEV charging demand on expressways is a complex and critical process involving various aspects of energy production, storage, distribution, and use. The key to solving this problem lies in using MESTs to establish suitable energy storage for PV generation and a dispatch system for expressways.

Over the past few years, the management of MESTs has received widespread attention from scholars (see Table 2). In essence, the MEST is a unique type of the MESS. Hence, the research on the MEST draws its foundation from the research on the MESS. At the beginning, Liang et al. developed a two-level optimization method for fixed and mobile energy storage, focusing on voltage offsets to enhance in-situ PV consumption capacity and cut down operational expenses [31]. The rise in reliability requirements for power systems has increased the demand for movable power-supply devices. Especially in areas frequented by natural disasters like earthquakes, fixed energy storage systems' role is significantly weaker than MESS. For example, Shi et al. investigated a stochastic planning model to reduce load loss by coordinating mobile emergency generators and the MESS [32]. However, the management and scheduling of MESS are crucial issues. To address this issue, scholars have utilized optimization algorithms like multi-objective augmented gray wolf optimizer [33], two-phase MESS scheduling method [34], and a load restoration strategy considering fixed and mobile energy storage systems [35], achieving good performance in handling large loads and high renewable resource penetration. As the application progresses, it reveals that relying on dispatch for power restoration can lead to high costs in cases of severe load inequalities or electricity technical issues [39]. Thus, strategies such as reducing electricity purchasing expenditure [40], improving distribution system resilience [36], collaborative optimization [37], rerouting MESS [38], and re-configuring the multi-benefit planning framework for MESS in active distribution systems [41] have been proposed. Among them, energy sharing using MESS at the community level is a promising idea for future research [42]. Then, Yao et al. proposed a rolling integrated service restoration strategy for urban roads using MEST fleets to reduce system costs [43]. The increasing demand for BEV charging facilities necessitates research on optimizing MESS scheduling and management in urban road scenarios. This guarantees the timely provision of sufficient power to charge BEVs.

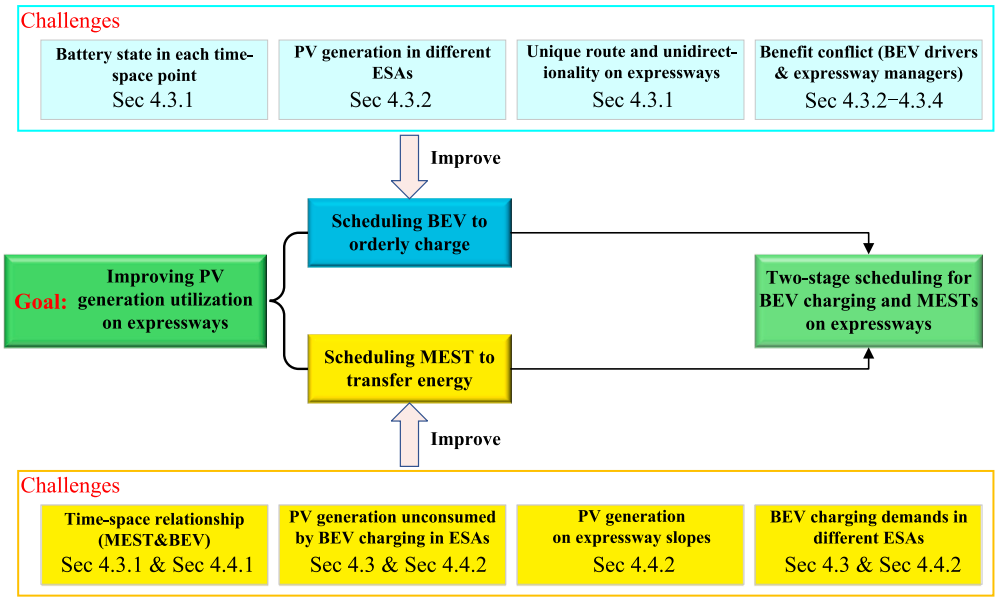


**Fig. 1.** Relationship between the key parts of this study.

Despite significant progress in MEST studies in urban areas, it remains challenging for these models to accurately characterize the wide spatial span of MEST on expressways. First of all, PV generation on expressways lacks transmission equipment and cannot be dispatched freely like urban roads, making MEST the only carrier capable of power dispatch and transmission. Secondly, factors such as weather conditions can influence the generation of solar energy sources like light, making them unstable and intermittent. Driving behavior, route, and battery level also influence the BEV's charging loads. Thirdly, expressways' high speed and congestion-free nature enable MEST to access energy supply/demand points for charging/discharging in a timely manner, addressing spatial and temporal uncertainty in PV generation. Previous studies have failed to illustrate the correlation between the spatial–temporal location of MEST and energy distribution.

### 2.3. Motivation

The analysis of existing literature reveals that optimizing the coupled relationship between BEV charging and MEST scheduling on expressways is a complex issue that requires further resolution. The main issues arise from the significant differences in transportation modes, application scenarios, design considerations, scale, layout, and economic benefits between urban roads and expressways. Our goal in this work is to fill the aforementioned gaps by presenting a meticulously designed mathematical model that is well-optimized for MEST dispatch to provide power for BEV charging. Unlike existing urban models, the proposed two-stage scheduling approach integrates a spatial–temporal network with expressway-energy characteristics for MESTs and BEVs to address geographic variations in PV generation, BEV battery levels, and the constraints of expressway travel. By utilizing MESTs for energy scheduling, this method resolves the issue of energy distribution across wide, isolated locations and unstable PV generation, which previous studies have failed to address. The study offers valuable insights into the intricate difficulties of the expressway manager integrating MEST management with the BEV charging plan. Fig. 1 illustrates the relationship between the key parts of this study.

## 3. Problem description

Fig. 2 shows the operation of BEVs and MESTs on expressways. In the intricate tapestry of energy transition, national and regional policies emerge as powerful catalysts, fervently championing the utilization of solar energy while simultaneously incentivizing robust infrastructure investments. This strategic alignment not only elevates the significance of expressway managers but also positions them as linchpins in the quest for sustainable energy solutions [44,45]. As a result, the proliferation of advanced information-sharing frameworks and cutting-edge energy management technologies further empowers these expressway managers, equipping them with the tools necessary to navigate the complexities of energy scheduling. Consequently, the expressway manager is envisioned as a cross-regional authority overseeing PV installations, MESTs, expressway entrances and exits, and EVCSs within ESAs. From an economic perspective, expressway managers stand to gain significantly by supplying energy to BEVs, thereby diminishing reliance on traditional power grids. This shift not only enhances financial returns but also fosters a more resilient energy model. Environmentally, the manager plays a crucial role in mitigating carbon emissions by optimizing the utilization of PV systems, thus contributing to a greener ecosystem.

In this context, ESAs have emerged as the preferred venues for constructing EVCSs, owing to their spatial advantages and strategic locations. By late 2024, a remarkable 97% of ESAs across China are equipped with EVCSs [46], underscoring their pivotal role in the electric mobility landscape. Consequently, this study posits that each EVCS is integrated within the ESA framework.

For operational efficiency, MESTs are designed to remain within the confines of the expressway, facilitating movement exclusively between ESAs. These MESTs execute U-turns through the corridors of the ESAs, enabling them to depart in two distinct directions. As previously discussed in Section 1, PV installations are strategically located within these ESAs, providing the necessary energy to support MEST operations. The synergy among MESTs, PV systems, and the grid within ESAs collectively powers the EVCSs. It is important to note that this study primarily focuses on the energy demands of EVCSs concerning BEV charging requirements. Other operational electricity needs, such as monitoring systems and equipment control, are intentionally excluded from the analysis to maintain clarity and specificity in addressing the core objectives of energy management.

Generally, expressway slopes are characterized by the absence of transmission lines and lower electricity demands, which complicates the integration and scheduling of PV generation in these areas. In practice, temporary parking areas have been established along expressways to accommodate large trucks, primarily addressing concerns

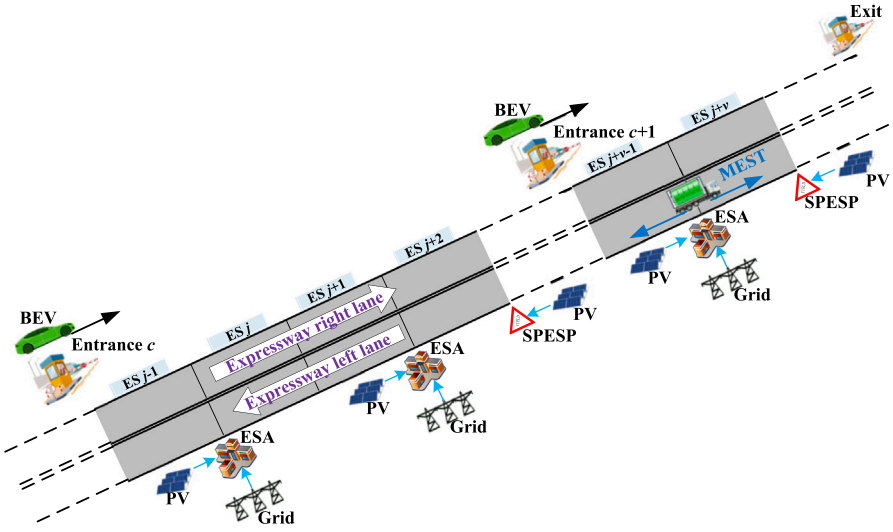


**Fig. 2.** Illustration of the operation of BEVs and MESTs on expressways.

such as tire and brake fatigue. Notably, some of these parking areas are situated near slopes where PV equipment is installed. This study posits that these temporary parking areas can serve as power supply points, designated as slope photovoltaic energy supply points (SPESPs), for connecting and utilizing slope-mounted PV systems. MESTs are permitted to park and charge at SPESPs. However, due to spatial constraints and the primary function of these areas to serve large trucks, expressway managers typically discourage BEVs from utilizing these locations for parking, citing safety concerns. Furthermore, the lack of power grid distribution surrounding SPESPs presents significant challenges in relying solely on PV generation to consistently meet BEV charging demands. As a result, investing in BEV charging infrastructure at SPESPs may not be economically viable for expressway managers. Consequently, these factors collectively lead to the prohibition of BEV charging at SPESPs.

This study splits the expressway into equidistant segments, with the index set of the expressway segment (ES) being defined as $J^{Set} = \{1, \ldots, J\}$. On opposite expressway directions, the one-way roadways are referred to as the left and right lanes, respectively. Notably, our modeling focuses solely on simulating BEV driving in the right lane. This study assumes that the expressway system model includes a single exit on ES $J$, with $c \in C^{Set}$ indexing the set of expressway entrances and $b \in B^{Set}$ indexing the set of BEVs. The set of BEVs entering expressways from entrance $c$ is defined by $B^c_{BEV}(B^c_{BEV} \subseteq B^{Set})$, while this study denotes the index set of ESs through which those BEVs will travel as $J^c_{BEV}(J^c_{BEV} \subseteq J^{Set})$. Furthermore, this study assumes each expressway entrance is positioned between adjacent ESs. With BEVs entering expressways from entrance $c$, this study defines the index of the first ES that these BEVs travel through as $j^c(j^c \in J^c_{BEV})$. This study defines that $n \in N^{Set}$ indexes the set of ESAs. The index set of BEVs entering expressways from entrances in front of ESA $n$ is denoted as $B^n_{BEV}(B^n_{BEV} \in B^{Set})$, and BEVs in this set are allowed to travel through ESA $n$. Moreover, this study assumes that MESTs cannot exit expressways. As a result, the moving range of MESTs on expressways is from ESA 1 to ESA $N$. The manager is expected to find it convenient to place all MESTs in ESAs during the initial and concluding time slots. Therefore, this study defines that $m \in M^{Set}$ indexes the set of MESTs. In the initial time slot, this study denotes the index set of MESTs in ESA $n$ as $M^n_{MEST}(M^n_{MEST} \subseteq M^{Set})$.

This study optimizes BEV charging schemes and schedules MESTs to improve the utilization of PV generation along expressways based on the above problem description.

Sets and indices

| | |
|---|---|
| $B^{Set}$, $b$ | Set and index of BEVs |
| $J^{Set}$, $j$ | Set and index of ESs |
| $C^{Set}$, $c$ | Set and index of expressway entrances |
| $T^{Set}$, $t$ | Set and index of time slots |
| $N^{Set}$, $n$ | Set and index of ESAs |
| $A^{Set}$, $a$ | Set and index of SPESPs |
| $M^{Set}$, $m$ | Set and index of MESTs |
| $K^{Set}$, $k$ | Set and index of BEV charging pricing options |
| $B^c_{BEV}$ | Set of BEVs entering expressways from entrance $c$ |
| $J^c_{BEV}$ | Set of ESs which BEVs entering expressways from entrance $c$ will travel through |
| $J_{MEST}$ | Set of ESs that MESTs are allowed to move |
| $J^{Set}_{ESA}$ | Set of space dimension of ESA spatial–temporal mesh |
| $J^{Set}_{SPESP}$ | Set of space dimension of SPESP spatial–temporal mesh |
| $B^n_{BEV}$ | Set of BEVs entering expressways from entrances in the front of ESA $n$ |
| $J^c_{ESA}$ | Set of ESA spatial–temporal meshes which BEVs entering from entrance $c$ can travel through |
| $M^n_{MEST}$ | Set of MESTs in the initial time slot in ESA $n$ |
| $j^n_{ESA}$ | Index of space dimension of spatial–temporal mesh in ESA $n$ |
| $j^a_{SPESP}$ | Index of space dimension of spatial–temporal mesh at SPESP $a$ |
| $j^c$ | Index of the first ES that BEVs travel through after entering expressways from entrance $c$ |

**Variables**

| | |
|---|---|
| $x^v_{j,t,b}$ | Binary variable indicating whether BEV $b$ selects ES spatial–temporal mesh (= 1 if being selected, = 0 otherwise) |
| $z^v_{j,t,b}$ | Binary variable indicating whether BEV $b$ is parked for the uncharged duration in ESA spatial–temporal mesh (= 1 if being parked, = 0 otherwise) |
| $y^v_{j,t,b}$ | Binary variable indicating whether BEV $b$ charges in ESA spatial–temporal mesh (= 1 if charging, = 0 otherwise) |
| $SOC^v_{t,b}$ | Battery SOC of BEV $b$ in time slot $t$ |
| $x^{er}_{j,t,m}$ | Binary variable indicating whether MEST $m$ selects ES spatial–temporal mesh when move in the right lane (= 1 if being selected, = 0 otherwise) |

| | |
|---|---|
| $x^{el}_{j,t,m}$ | Binary variable indicating whether MEST $m$ selects ES spatial–temporal mesh when move in the left lane (= 1 if being selected, = 0 otherwise) |
| $y^{ech}_{j,t,m}$ | Binary variable indicating whether MEST $m$ charges in ESA/SPESP spatial–temporal mesh (= 1 if charging, = 0 otherwise) |
| $y^{edis}_{j,t,m}$ | Binary variable indicating whether MEST $m$ discharges in ESA spatial–temporal mesh (= 1 if discharging, = 0 otherwise) |
| $z^{e}_{j,t,m}$ | Binary variable indicating whether MEST $m$ stay in ESA/SPESP spatial–temporal mesh (= 1 if staying, = 0 otherwise) |
| $p^{edis}_{j,t,m}$ | Discharging power for MEST $m$ in ESA spatial–temporal mesh |
| $p^{ech}_{j,t,m}$ | Charging power for MEST $m$ in ESA/SPESP spatial–temporal mesh |
| $SOC^{e}_{t,m}$ | SOC of BESD for MEST $m$ in time slot $t$ |
| $P^{g}_{n,t}$ | Power from the grid in time slot $t$ in ESA $n$ |
| $I^{EM}_{n,t,k}$ | Binary variable indicating whether to select charging price $\beta^{EM}_{n,t,k}$ (= 1 if being selected, = 0 otherwise) |

**Parameters**

| | |
|---|---|
| $J$ | Number of ESs |
| $C$ | Number of expressway entrances |
| $B$ | Number of BEVs |
| $N$ | Number of ESAs |
| $M$ | Number of MESTs |
| $T$ | Number of time slots |
| $A$ | Number of SPESPs |
| $K$ | Number of charging pricing options for BEVs |
| $E^{c}_{b}$ | Starting battery level for BEV $b$ entering expressways from entrance $c$ |
| $E^{max}_{BEV}$ | Battery volume for BEVs |
| $SOC^{min}_{BEV}$ | Minimum SOC for BEVs |
| $\omega^{+}$ | Charging power for each BEV in every time slot |
| $\omega^{-}$ | Battery energy consumption for each BEV in every ES spatial–temporal mesh |
| $\Delta t$ | Time slot length, which is 0.5 h in this paper |
| $\alpha^{e}_{n}$ | Number of MESTs in the initial time slot in ESA $n$ |
| $\alpha^{lim}_{ech}$, $\alpha^{lim}_{edis}$ | Maximum Charging and discharging number for MESTs |
| $E^{e}_{m}$ | Initial BESD level for MEST $m$ |
| $P^{max}_{ech}$, $P^{max}_{edis}$ | Maximum charging and discharging power for each MEST |
| $E^{max}_{MEST}$ | BESD volume for each MEST |
| $SOC^{min}_{MEST}$ | Minimum SOC of BESD for MESTs |
| $\beta^{EM}_{n,t,k}$ | Charging price choice $k$ for BEVs in ESA $n$ in time slot $t$ |
| $\beta^{z}_{BEV}$ | Parking fees for BEVs in ESAs in one time slot (uncharged period) |
| $\beta^{g}_{n,t}$ | Electric energy price of the grid in ESA $n$ during time slot $t$ |
| $P^{max}_{n}$ | BEV charging load limit for the EVCS in ESA $n$ |
| $P^{PV}_{n,t}$ | PV generation in ESA $n$ during time slot $t$ |
| $P^{unPV,first*}_{n,t}$ | Unconsumed PV generation in ESA $n$ during time slot $t$ in the first stage |
| $P^{PV}_{a,t}$ | PV generation at SPESP $a$ during time slot $t$ |
| $E^{max}_{EM}$ | Maximum income of the expressway manager for the operation duration |
| $\beta^{avg}_{n}$ | Maximum average price for BEV charging in ESA $n$ |
| $\alpha^{zlim}_{b}$ | Maximum overall parking time for BEV $b$ during its uncharged period |
| $\beta^{vtime}$ | Temporal cost of BEV parking indicating the quantified time expenditure of BEV drivers during their uncharged period |
| $v^{ep}$ | Moving expense per ES for every MEST |
| $v^{ech}$, $v^{edis}$ | Charging and discharging degradation expenses of BESD for every MEST |

## 4. Methodology

In this section, the general description of the two-stage scheduling method is first introduced. The spatial–temporal network model for BEVs and MESTs is then presented. Next, the BEV charging scheduling method in the first stage and the MEST scheduling method in the second stage are illustrated in detail.

### 4.1. General description of two-stage scheduling method

Fig. 3 illustrates the structure of the proposed two-stage scheduling method. Due to business deals with the electrical sector, the expressway manager is assumed to acquire the day-ahead locational marginal prices (LMP) and PV generation [47]. The assumption is made that BEV drivers utilize vehicle-to-network technology to provide data regarding their expressway itinerary and battery states [48]. Subsequently, the expressway manager sends charging plans to BEV drivers. This study presumes that BEV drivers adhere to these charging plans recommended by the expressway manager. In the first stage, based on the above data, the expressway manager determines the charging schemes of BEVs and pricing options in ESAs. To ensure that BEVs' benefits are considered, the problem in the first stage is formulated as a two-layer optimization model. The upper-layer model optimizes BEV charging and pricing plans, whereas the lower-layer model aims to reduce BEV drivers' parking and charging costs. Actually, drivers may choose to park their BEVs in ESAs for a variety of reasons, and they may perceive the parking time as a cost. Hence, this study devises an expense function for BEV drivers that takes into account the parking time during the uncharged period and the associated charging expenses. The lower-layer model employs this expense function to characterize the benefits for BEV drivers. The interacting process between the upper and lower layers is denoted as the results of the upper-level model that should meet minimum charging and parking expenses. Every BEV driver has a plethora of options when it comes to charging schemes; therefore, it can be challenging to integrate all viable solutions from the lower-layer model as constraints in the upper-layer model. To tackle this two-layer model, this study utilizes a C&CG method. Subsequently, data on BEV charging loads supplied by the grid and the unconsumed PV generation in every ESA obtained in the first stage is forward to the problem in the second stage. The expressway manager can dispatch MESTs to rich energy regions with lower electricity demands to store energy, taking into account the unconsumed PV generation along expressways. BEV charging loads make it challenging for the PV generation in ESAs to meet energy demands. Furthermore, the expressway manager can enhance its economic and environmental benefits by deploying MESTs with PV-generating energy to ESAs with higher charging loads. Additionally, SPESPs do not provide a location for BEV charging. To store PV generation, the expressway manager should dispatch MESTs to SPESPs. Based on the first-stage calculation, the second-stage problem is to find the best way to schedule MESTs so that they make the most money while taking into account LMP, PV generation on slopes, and the costs of movement and BESD degradation.

### 4.2. General description of spatial–temporal network model

This study develops a spatial–temporal network model in order to depict the transportation and energy characteristics of BEVs and MESTs on expressways. Unlike urban transportation, MESTs and BEVs have the following main characteristics on expressways:

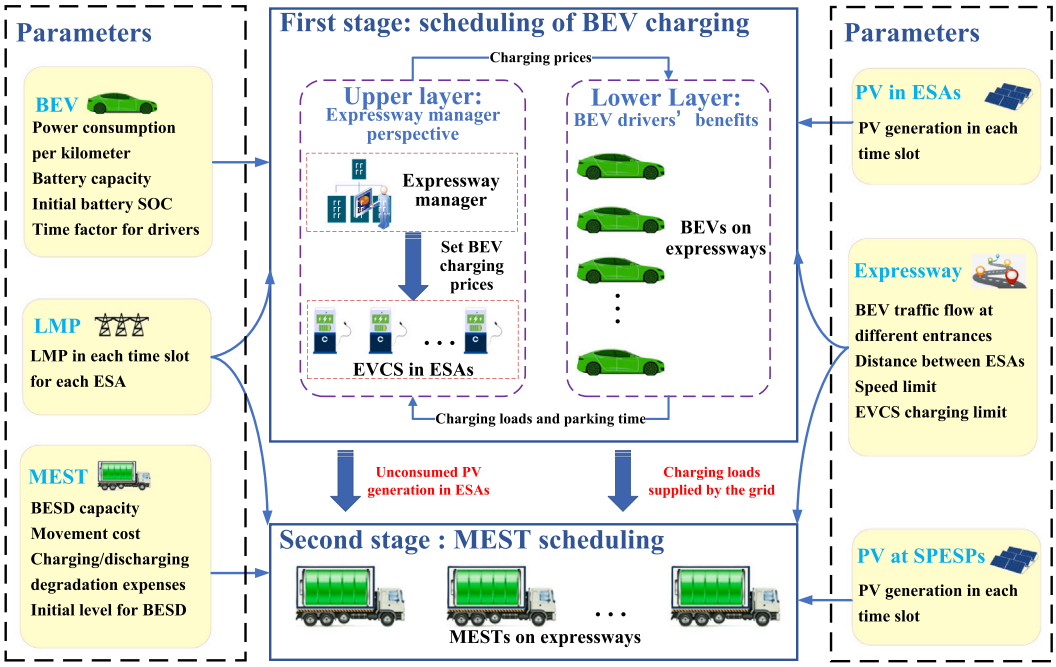


**Fig. 3.** Structure of the proposed two-stage scheduling method.

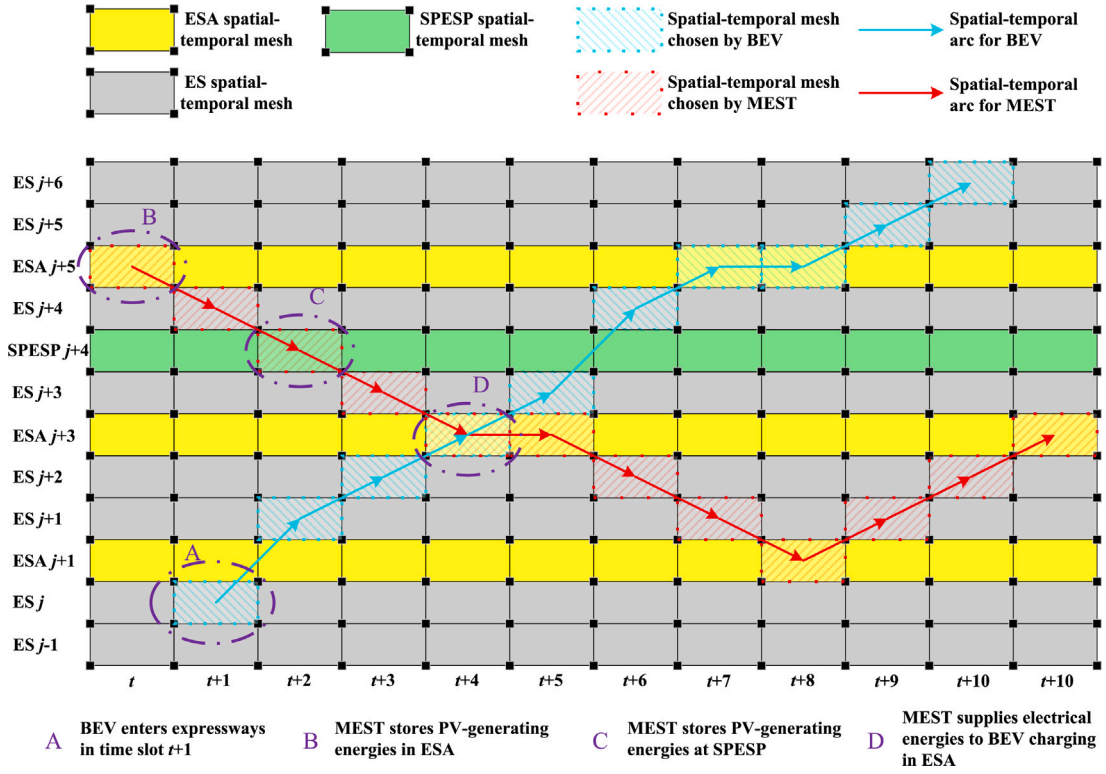


**Fig. 4.** Illustration of the spatial–temporal network.

(1) On expressways, the BEV's origin–destination pair has only one optional route scheme.
(2) MESTs cannot leave the expressway transportation system. This implies that MESTs can only move between ESAs.
(3) Generally, expressways have high velocity and are non-cong ested. The average speed at which MESTs and BEVs travel is restricted by the expressway speed constraint.

To describe these characteristics, three types of spatial–temporal meshes are proposed, including ES spatial–temporal meshes (light gray boxes), SPESP spatial–temporal meshes (light green boxes), and ESA spatial–temporal meshes (light yellow boxes), as shown in Tables 3–4. Fig. 4 shows the spatial–temporal network for MESTs and BEVs. Specifically, an ES spatial–temporal mesh indicates the movement of MEST or BEV through an ES, whereas ESA spatial–temporal meshes show the electricity-energy exchange of MESTs and BEVs in ESAs, and SPESP

**Table 3**
General description of three types of spatial–temporal meshes for BEVs.

| Category | Consuming battery energy | Charging for battery | Parking | Space dimension index | Time dimension index |
|---|---|---|---|---|---|
| ES spatial–temporal mesh | Yes | No | No | $j$ | $t$ |
| ESA spatial–temporal mesh | No | Yes | Yes | $j^n_{ESA}$ | $t$ |
| SPESP spatial–temporal mesh | No | No | No | $j^a_{SPESP}$ | $t$ |

**Table 4**
General description of three types of spatial–temporal meshes for MESTs.

| Category | Charging for BESD | Discharging for BESD | Staying | Space dimension index | Time dimension index |
|---|---|---|---|---|---|
| ES spatial–temporal mesh | No | No | No | $j$ | $t$ |
| ESA spatial–temporal mesh | Yes | Yes | Yes | $j^n_{ESA}$ | $t$ |
| SPESP spatial–temporal mesh | Yes | Yes | Yes | $j^a_{SPESP}$ | $t$ |

spatial–temporal meshes describe MEST energy extraction from sloped PV installations. As mentioned above, expressways are typically high-velocity and non-congested, meaning that vehicles generally cover the same distance in the same amount of time. To simplify the model, this study assumes that MESTs and BEVs travel at the same speed on expressways and can move through an ES in one time slot. For convenience, this study assumes that the spatial dimension of an ES spatial–temporal mesh is indexed in the same way as the ES segments defined in Section 3. Therefore, when a MEST or BEV selects an ES spatial–temporal mesh, it indicates the vehicle travels through an ES. To further simplify, this study assume that adjacent ESAs are separated by two ESs. The element in the set $J^{Set}_{ESA}(J^{Set}_{ESA} \subseteq J^{Set})$ indexes the space dimension for each ESA spatial–temporal mesh. $j^n_{ESA}$ $(j^n_{ESA} \in J^{Set}_{ESA})$ indexes the space dimension of the spatial–temporal mesh in ESA $n$. In practice, the setting of SPESPs is based on the distribution of slope PV installations and the situation of expressways. For instance, the SPESP in Fig. 4 is assumed to be set between ES $j+3$ and $j+4$, whereas its index of the space dimension is $j+4$. This study defines that the element in set $J^{Set}_{SPESP}(J^{Set}_{SPESP} \subseteq J^{Set})$ indexes the space dimension for each SPESP spatial–temporal mesh.

BEVs consume their cell energy when the ES spatial–temporal mesh is selected. Each ES spatial–temporal mesh corresponds to a consistent expressway distance in space, implying the same energy consumption for BEVs choosing these meshes. The choice of an ESA spatial–temporal mesh implies that BEVs will be engaged in charging and parking behavior in the ESA. In Fig. 4, the blue arrow indicates the spatial–temporal arc for the BEV, whereas the light blue dotted box depicts the spatial–temporal mesh chosen by the BEV. It can be seen that a BEV enters expressways from an entrance located between ES $j-1$ and ES $j$. It does not enter ESA $j+1$ and instead moves directly from ES $j$ to ES $j+1$. Then, it passes ES $j+2$ and enters ESA $j+3$ for charging. Furthermore, MESTs are assumed to use ES spatial–temporal meshes without consuming energy, whereas ESA spatial–temporal meshes represent their energy exchange behavior, staying in ESA, and performing U-turns. MESTs choosing SPESP spatial–temporal meshes represent their charging or staying in this SPESP. In Fig. 4, the red arrow represents the MEST's spatial–temporal arc, whereas the red dotted box represents the chosen spatial–temporal mesh. In ESA $j+5$, an MEST stays in time slot $t$. By choosing ES spatial–temporal mesh $j+4$, the MEST moves into SPESP $j+4$ for charging. Next, it moves into ESA $j+3$ for supplying BEV charging. It is noticed that this MEST executes a U-turn in ESA $j+1$.

### 4.3. BEVs charging scheduling in the first stage

The charging plans and prices for BEVs in the first stage are optimized based on PV generation, LMP, and BEV drivers' information. Specifically, the formulation of a spatial–temporal network model for BEVs portrays the coupled relationship between battery energy and spatial–temporal locations. The structure of the two-layer optimization model ensures the benefit of BEV drivers while generating charging loads in each ESA.

#### 4.3.1. Formulation of spatial–temporal network model for battery electric vehicles

The coupling relationship between time-space and energy in BEVs is described using three types of binary variables and one type of continuous variable. The binary variable $x^v_{j,t,b}$ indicates whether BEV $b$ passes through ES $j$ in time slot $t$. Eq. (1) indicates BEV $b$ moves into expressways from entrance $c$ in time slot $t$. Eq. (2) defines the state shift between two neighboring ES spatial–temporal meshes for BEVs. This state shift eliminates the potential for BEVs to move through ESAs, leading to the denotation of $j : \{j \in J^{Set} | j \notin J^{Set}_{ESA}\}$ in Eq. (2). Moreover, Eqs. (2)–(3) have a coupled impact that ensures each BEV route is unique and unidirectional. The binary variable $y^v_{j,t,b}$ indicates whether BEV $b$ charges in ESA $j$. The binary variable $z^v_{j,t,b}$ indicates whether BEV $b$ is parked in ESA $j$ during the uncharged period. Eq. (4) defines how BEVs shift their states when moving through ESAs. The unique state in every time slot for BEVs that enter from entrance $c$ is guaranteed by Eq. (5).

$$x^v_{j^c,t,b} = 1 \quad \forall j^c \in J^c_{BEV},\ t \in T^{Set},\ b \in B^c_{BEV} \tag{1}$$

$$x^v_{j-1,t-1,b} = x^v_{j,t,b} \quad \forall t \in T^{Set},\ b \in B^c_{BEV} \tag{2}$$

$$\sum_{t=1}^{T} x^v_{j,t,b} = 1 \quad \forall j \in J^{Set},\ b \in B^{Set} \tag{3}$$

$$x^v_{j-1,t-1,b} + y^v_{j,t-1,b} + z^v_{j,t-1,b} = x^v_{j,t,b} + y^v_{j,t,b} + z^v_{j,t,b} \quad \forall j \in J^{Set}_{ESA},\ t \in T^{Set},\ b \in B^{Set} \tag{4}$$

$$\sum_{j \in J^c_{BEV}} x^v_{j,t,b} + \sum_{j \in J^c_{ESA}} y^v_{j,t,b} + \sum_{j \in J^c_{ESA}} z^v_{j,t,b} = 1 \quad \forall t \in T^{Set},\ b \in B^c_{BEV} \tag{5}$$

The continuous variable $SOC^v_{t,b}$ indicates state-of-charge (SOC) for the BEV's battery. $E^{max}_{BEV}$ indicates the maximum battery volume. Eq. (6) defines the starting SOC for BEVs entering expressways from entrance $c$ in time slot $t$. Eq. (7) determines the SOC change for BEVs in every time slot. In this scenario, it is assumed that every BEV has the same charging power. The parameter $\omega^+$ in Eq. (7) indicates charging power for each BEV. Eq. (8) restricts the minimum SOC for BEVs.

$$SOC^v_{t,b} = \frac{E^c_b}{E^{max}_{BEV}} \quad \forall c \in C^{Set},\ b \in B^{Set},\ t \in T^{Set} \tag{6}$$

$$SOC^v_{t,b} \cdot E^{max}_{BEV} = SOC^v_{t-1,b} \cdot E^{max}_{BEV} + \omega^+ \cdot \Delta t \cdot \sum_{j \in J^c_{ESA}} y^v_{j,t,b} - \omega^- \cdot \sum_{j \in J^c_{BEV}} x^v_{j,t,b} \quad \forall c \in C^{Set},\ b \in B^c_{BEV},\ t \in T^{Set} \tag{7}$$

$$SOC^{min}_{BEV} \le SOC^v_{t,b} \quad \forall t \in T^{Set},\ b \in B^{Set} \tag{8}$$

#### 4.3.2. Upper-layer model

The objective of the upper layer model is determined by the perspective of the expressway manager, aiming to maximize the net earnings in Eq. (9). In detail, the first term of Eq. (9) considers all income generated from electricity supply for BEV charging in ESAs. The EVCS manager charges parking fees for BEVs left uncharged, resulting in revenue for the expressway manager [49], as shown in the second term of Eq. (9). The total cost paid by the expressway manager in obtaining electric energy from the grid is depicted in the third term of Eq. (9), where $P^{g}_{n,t}$ represents the power from the grid in time slot $t$ in ESA $n$. Moreover, auxiliary variables $E^{bc}_{n,t,k}$ and $E^{z}_{n,t}$ are introduced. They are continuous variables, and their detailed expressions are presented in Eqs. (10)–(11). $E^{bc}_{n,t,k}$ represents the income of supplying electricity during time slot $t$ in ESA $n$ if the expressway manager opts for pricing choice $k$ of BEV charging. Continuous variable $W^{bc}_{n,t}$ indicates the BEV charging demands during time slot $t$ in ESA $n$. $E^{z}_{n,t}$ denotes that the expressway manager obtains parking fees from BEVs during time slot $t$ in ESA $n$.

$$\max \sum_{t=1}^{T}\sum_{n=1}^{N}\sum_{k=1}^{K} E^{bc}_{n,t,k} + \sum_{t=1}^{T}\sum_{n=1}^{N} E^{z}_{n,t} - \sum_{t=1}^{T}\sum_{n=1}^{N} \beta^{g}_{n,t}\cdot P^{g}_{n,t}\cdot \Delta t \tag{9}$$

$$E^{bc}_{n,t,k} = \beta^{EM}_{n,t,k}\cdot W^{bc}_{n,t}\cdot I^{EM}_{n,t,k},\ W^{bc}_{n,t} = \omega^{+}\cdot\Delta t\cdot \sum_{b\in B^{n}_{BEV}} y^{v}_{j^{n}_{ESA},t,b}$$
$$\forall n\in N^{Set},\ t\in T^{Set},\ k\in K^{Set} \tag{10}$$

$$E^{z}_{n,t} = \sum_{b\in B^{n}_{BEV}} \beta^{z}_{BEV}\cdot\Delta t\cdot z^{v}_{j^{n}_{ESA},t,b} \quad \forall n\in N^{Set},\ t\in T^{Set} \tag{11}$$

In general, a few factors (such as the number of charging piles, available parking spaces, and inverter capacity) restrict an EVCS's capacity to provide BEV charging. As a result, BEV charging loads in ESA $n$ during time slot $t$ are restricted by Eq. (12).

$$\omega^{+}\cdot \sum_{b\in B^{n}_{BEV}} y^{v}_{j^{n}_{ESA},t,b} \le P^{max}_{n} \quad \forall n\in N^{Set},\ T^{Set} \tag{12}$$

Note that $E^{bc}_{n,t,k}$ in Eq. (9) is nonlinear. Therefore, the McCormick Envelop is employed to transform this auxiliary variable into a linear form, as demonstrated by the following constraints:

$$E^{bc}_{n,t,k} \le \beta^{EM}_{n,t,k}\cdot W^{bc}_{n,t} \quad \forall n\in N^{Set},\ t\in T^{Set},\ k\in K^{Set} \tag{13}$$

$$E^{bc}_{n,t,k} \le \beta^{EM}_{n,t,k}\cdot P^{max}_{n}\cdot\Delta t\cdot I^{EM}_{n,t,k} \quad \forall n\in N^{Set},\ t\in T^{Set},\ k\in K^{Set} \tag{14}$$

$$E^{bc}_{n,t,k} \ge \beta^{EM}_{n,t,k}\cdot P^{max}_{n}\cdot\Delta t\cdot I^{EM}_{n,t,k} + \beta^{EM}_{n,t,k}\cdot W^{bc}_{n,t} + \beta^{EM}_{n,t,k}\cdot P^{max}_{n}\cdot\Delta t$$
$$\forall n\in N^{Set},\ t\in T^{Set},\ k\in K^{Set} \tag{15}$$

Regarding the pricing for BEV charging, this study adopts the strategy in the literature [11], which decides pricing schemes for BEV charging in each time-space location among a specific number of candidates for prices. The disparities in charging costs in different ESAs during different time slots can be clearly shown for BEV drivers by using this pricing strategy for BEV charging. As illustrated in Eq. (16), a series of binary variables are introduced to indicate whether to choose a certain pricing option for the target EVCS in a specific time slot.

$$\sum_{k=1}^{K} I^{EM}_{n,t,k} = 1 \quad \forall n\in N^{Set},\ t\in T^{Set} \tag{16}$$

Eq. (17) enforces that the combined power supply from PV generation and the grid is enough to charge BEVs in ESA $n$ in time slot $t$. To prevent excessive charges, this study introduces two capping constraints for the expressway manager, as illustrated in Eqs. (18)–(19), considering it as a monopolistic enterprise. $E^{max}_{EM}$ denotes the expressway manager's maximum income. $\beta^{avg}_{n}$ indicates the maximum average price for BEV charging in ESA $n$. Furthermore, Eq. (20) restricts the maximum overall parking time for BEV $b$ during its uncharged period.

$$P^{g}_{n,t} + P^{PV}_{n,t} \ge \omega^{+}\cdot \sum_{b\in B^{n}_{BEV}} y^{v}_{j^{n}_{ESA},t,b} \quad \forall n\in N^{Set},\ t\in T^{Set} \tag{17}$$

$$\sum_{t=1}^{T}\sum_{n=1}^{N}\sum_{k=1}^{K} E^{bc}_{n,t,k} + \sum_{t=1}^{T}\sum_{n=1}^{N} E^{z}_{n,t} \le E^{max}_{EM} \tag{18}$$

$$\frac{1}{T}\cdot\sum_{t=1}^{T}\sum_{k=1}^{K} \beta^{EM}_{n,t,k}\cdot I^{EM}_{n,t,k} \le \beta^{avg}_{n} \quad \forall n\in N^{Set} \tag{19}$$

$$\sum_{j\in J^{c}_{ESA}}\sum_{t\in T^{Set}} z^{v}_{j,t,b} \le \alpha^{zlim}_{b} \quad \forall c\in C^{Set},\ b\in B^{c}_{BEV} \tag{20}$$

#### 4.3.3. Lower-layer model

This study develops a parking and charging expense function for BEV drivers on expressways, with the lower-layer model aiming to minimize this expense function, as depicted in Eq. (21). BEV drivers may need to park in the ESA during non-charging periods as a temporal cost. For ease of calculation, this time cost is converted into a measurable value based on the average hourly wage [50]. Without loss of generality, all ESAs in this study are assumed to have the same measurable value for temporal costs. The auxiliary variable $E^{vtime}_{n,t}$ quantifies the temporal cost of BEV drivers for uncharged duration, and the detailed expression is shown in Eq. (22). The parameter $\beta^{vtime}$ in Eq. (22) denotes the temporal cost for each time slot as evaluated by BEV drivers in each ESA. Additionally, in Eq. (21), $E^{bc}_{n,t,k}$ represents BEV drivers' expenses for battery charging, whereas $E^{z}_{n,t}$ stands for their expenses for parking. The detailed expressions for $E^{bc}_{n,t,k}$ and $E^{z}_{n,t}$ are provided in Eqs. ((10))-((11)).

$$\min \sum_{t=1}^{T}\sum_{n=1}^{N} E^{vtime}_{n,t} + \sum_{t=1}^{T}\sum_{n=1}^{N}\sum_{k=1}^{K} E^{bc}_{n,t,k} + \sum_{t=1}^{T}\sum_{n=1}^{N} E^{z}_{n,t} \tag{21}$$

$$E^{vtime}_{n,t} = \sum_{b\in B^{n}_{BEV}} \beta^{vtime}\cdot z^{v}_{j^{n}_{ESA},t,b}\cdot\Delta t \quad \forall n\in N^{Set},\ t\in T^{Set} \tag{22}$$

#### 4.3.4. Solution approach for the first stage

The upper-layer model should consider minimizing charging and parking expenses for BEV drivers when planning BEV charging. Hence, the first stage is built as a bi-level mixed integer linear programming (BiMIP).

$$\max \sum_{t=1}^{T}\sum_{n=1}^{N}\sum_{k=1}^{K} E^{bc}_{n,t,k} + \sum_{t=1}^{T}\sum_{n=1}^{N} E^{z}_{n,t} - \sum_{t=1}^{T}\sum_{n=1}^{N} \beta^{g}_{n,t}\cdot P^{g}_{n,t}\cdot\Delta t$$
s.t.(1)–(8), (10) – (20)

$$x^{v}_{j,t,b},\ z^{v}_{j,t,b},\ y^{v}_{j,t,b},\ E^{bc}_{n,t,k} \in \operatorname{argmin} \sum_{t=1}^{T}\sum_{n=1}^{N} E^{vtime}_{n,t} + \sum_{t=1}^{T}\sum_{n=1}^{N}\sum_{k=1}^{K} E^{bc}_{n,t,k} + \sum_{t=1}^{T}\sum_{n=1}^{N} E^{z}_{n,t}$$
$$s.t.\quad (1)–(8),\ (10)–(11),\ (12)–(15),\ (20),\ (22)$$

This study solves the BiMIP model using the C&CG method [51], involving iterations to create variables and constraints for the upper-layer model to interact with the low-layer model. The main problem (MP) is the upper-layer model, which integrates an expanded constraint-variable set into every iteration via the Karush-Kuhn–Tucker condition. The MP is solved to find workable solutions and refresh the upper bound (UB), as illustrated in Eq. (23). The KKT condition is effectuated by dual variables $\mu_{n,t,1}$, $\mu_{n,t,2}$, $\mu_{n,t,3}$, $\mu_{n,t,4}$, and $\mu_{n,t,5}$. All dual variables are greater than or equal to 0. Notably, the variable $h$ in Eq. (23) indicates the iteration number. At iteration 0, Eqs. (23a)–(23i) should be excluded. The MP is iteratively solved until convergence is reached, adding Eqs. (23a)–(23i) as it goes. Moreover, the Big-M approach is used to transform the nonlinear constraints in Eqs. (23e)–(23h). **Algorithm 1** provides the detailed algorithmic procedures of the proposed C&CG method for solving the BiMIP model.

**Algorithm 1: The C&CG algorithm for the proposed BiMIP**

**Initialization:** Set iteration index $h = 0$, UB(0)=$+\infty$, LB(0)=$-\infty$
**while** $\frac{\mathrm{UB}(h)-\mathrm{LB}(h)}{\mathrm{LB}(h)} > \eta$ **do**
  **MP solving:** Obtain the optimal solution $\left(E^{bc,*}_{n,t,k}, \ldots, I^{EM,*}_{n,t,k},\ P^{g,*}_{n,t}\right)$ and $\Theta^*$
  **Update:** UB($h$)=$\Theta^*$
  **SP1 solving:** Given$\left(I^{EM,*}_{n,t,k},\ P^{g,*}_{n,t}\right)$ from the MP, obtain an optimal solution $\xi^*_I$
  **SP2 solving:** Given$\left(I^{EM,*}_{n,t,k},\ P^{g,*}_{n,t}\right)$ from the MP and $\xi^*_I$ from the SP1, obtain the optimal solution $\xi^*_{II}$ and $\left(x^{v,*}_{j,t,b},\ z^{v,*}_{j,t,b},\ y^{v,*}_{j,t,b}\right)$
  **Update:** LB($h$)=max$\left\{\mathrm{LB}(h),\ \xi^*_{II} - \sum_{t=1}^{T}\sum_{n=1}^{N}\beta^{g}_{n,t}\cdot P^{g,*}_{n,t}\cdot\Delta t\right\}$
  **Set:** $\left(x^{v,h+1}_{j,t,b}, y^{v,h+1}_{j,t,b}, z^{v,h+1}_{j,t,b}\right) = \left(x^{v,*}_{j,t,k}, y^{v,*}_{j,t,k}, z^{v,*}_{j,t,k}\right)$
  **Generate variables and constraints:** $\left(E^{bc,h+1}_{n,t,k}, \mu^{h+1}_{n,t,1}, \mu^{h+1}_{n,t,2}, \mu^{h+1}_{n,t,3}, \mu^{l+1}_{n,t,4}, \mu^{h+1}_{n,t,5}\right)$ and Eqs. (23a)–(23i), and then add them to the MP;
  **Update:** $h = h + 1$
**end while**

$$
\mathrm{MP}:\begin{cases}
\Theta = \max\ (9)\\
s.t.\ (1)\text{–}(8),\ (10)-(20)\\
\sum_{t=1}^{T}\sum_{n=1}^{N}E^{vtime}_{n,t}+\sum_{t=1}^{T}\sum_{n=1}^{N}\sum_{k=1}^{K}E^{bc}_{n,t,k}+\sum_{t=1}^{T}\sum_{n=1}^{N}E^{z}_{n,t}\\
\quad\le\sum_{t=1}^{T}\sum_{n=1}^{N}E^{vtime,h}_{n,t}+\sum_{t=1}^{T}\sum_{n=1}^{N}\sum_{k=1}^{K}E^{bc,h}_{n,t,k}+\sum_{t=1}^{T}\sum_{n=1}^{N}E^{z,h}_{n,t} \quad (a)\\
\sum_{t=1}^{T}\sum_{n=1}^{N}\sum_{k=1}^{K}E^{bc,h}_{n,t,k}+\sum_{t=1}^{T}\sum_{n=1}^{N}E^{z,h}_{n,t}\le E^{max}_{EM} \quad (b)\\
E^{bc,h}_{n,t,k}\le\beta^{EM}_{n,t,k}\cdot P^{max}_{n}\cdot\Delta t\cdot I^{EM,h}_{n,t,k},\ E^{bc,h}_{n,t,k}\le\beta^{EM}_{n,t,k}\cdot W^{bc,h}_{n,t}\\
\quad\forall n\in N^{Set},\ t\in T^{Set},\ k\in K^{Set} \quad (c)\\
E^{bc,h}_{n,t,k}\ge\beta^{EM}_{n,t,k}\cdot P^{max}_{n}\cdot\Delta t\cdot I^{EM,h}_{n,t,k}+\beta^{EM}_{n,t,k}\cdot W^{bc,h}_{n,t}+\beta^{EM}_{n,t,k}\cdot P^{max}_{n}\cdot\Delta t\\
\quad\forall n\in N^{Set},\ t\in T^{Set},\ k\in K^{Set} \quad (d)\\
\left(E^{bc,h}_{n,t,k}-\beta^{EM}_{n,t,k}\cdot P^{max}_{n}\cdot\Delta t\cdot I^{EM,h}_{n,t,k}-\beta^{EM}_{n,t,k}\cdot W^{bc,h}_{n,t}\right.\\
\quad\left.-\beta^{EM}_{n,t,k}\cdot P^{max}_{n}\cdot\Delta t\right)\cdot\mu^{h}_{n,t,1}=0\quad\forall n\in N^{Set},\ t\in T^{Set},\ k\in K^{Set} \quad (e)\\
\left(\beta^{EM}_{n,t,k}\cdot P^{max}_{n}\cdot\Delta t\cdot I^{EM,h}_{n,t,k}-E^{bc,h}_{n,t,k}\right)\cdot\mu^{h}_{n,t,2}=0,\\
\left(\beta^{EM}_{n,t,k}\cdot W^{bc,h}_{n,t}-E^{bc,h}_{n,t,k}\right)\cdot\mu^{h}_{n,t,3}=0\quad\forall n\in N^{Set},\ t\in T^{Set},\\
k\in K^{Set} \quad (f)\\
\left(E^{max}_{EM}-\sum_{t\in T^{Set}}\sum_{n\in N^{Set}}\sum_{k\in K^{Set}}E^{bc,h}_{n,t,k}-\sum_{t\in T^{Set}}\sum_{n\in N^{Set}}E^{z,h}_{n,t}\right)\cdot\mu^{h}_{n,t,4}=0,\\
\left(1-\mu^{h}_{n,t,1}+\mu^{h}_{n,t,2}+\mu^{h}_{n,t,3}+\mu^{h}_{n,t,4}\right)\cdot\mu^{h}_{n,t,5}=0\quad\forall n\in N^{Set},\ t\in T^{Set} \quad (g)\\
E^{cb,h}_{n,t,k}\cdot\mu^{h}_{n,t,5}=0\quad\forall n\in N^{Set},\ t\in T^{Set},\ k\in K^{Set} \quad (h)\\
1-\mu^{h}_{n,t,1}+\mu^{h}_{n,t,2}+\mu^{h}_{n,t,3}+\mu^{h}_{n,t,4}\ge 0\quad\forall n\in N^{Set},\ t\in T^{Set} \quad (i)
\end{cases}
\tag{23}
$$

The sub-problem (SP) is decomposed into two MILP problems, i.e., SP1 and SP2, with the lower-layer model being defined in Section 4.3.3. According to the optimal solution of the MP, the SP1 determines the minimum expenses $\xi^*_I$ for BEV drivers. Then, based on $\xi^*_I$ and the MP's results, the SP2 is solved to acquire $\left(x^{v,*}_{j,t,k}, y^{v,*}_{j,t,k}, z^{v,*}_{j,t,k}\right)$. The detailed expressions for SP1 and SP2 are listed as follows.

$$
\mathrm{SP1}:\begin{cases}
\xi_I = \min\ (21)\\
s.t.\ (1)\text{–}(8),\ (10)-(13),\ (20),\ (22)\\
E^{bc}_{n,t,k}\le\beta^{EM}_{n,t,k}\cdot P^{max}_{n}\cdot\Delta t\cdot I^{EM,*}_{n,t,k}\quad\forall n\in N^{Set},\\
\quad\times\in T^{Set},\ k\in K^{Set} \quad (a)\\
E^{bc}_{n,t,k}\ge\beta^{EM}_{n,t,k}\cdot P^{max}_{n}\cdot\Delta t\cdot I^{EM,*}_{n,t,k}+\beta^{EM}_{n,t,k}\cdot W^{bc}_{n,t}\\
\quad+\beta^{EM}_{n,t,k}\cdot P^{max}_{n}\cdot\Delta t\quad\forall n\in N^{Set},\ t\in T^{Set},\ k\in K^{Set} \quad (b)
\end{cases}
\tag{24}
$$

$$
\mathrm{SP2}:\begin{cases}
\xi_{II} = \max\ \sum_{t=1}^{T}\sum_{n=1}^{N}\sum_{k=1}^{K}E^{bc}_{n,t,k}+\sum_{t=1}^{T}\sum_{n=1}^{N}E^{z}_{n,t}\\
s.t.\ (1)\text{–}(8),\ (10)-(13),\ (20),\ (22),\ (24),\ (24)\\
\sum_{t=1}^{T}\sum_{n=1}^{N}E^{vtime}_{n,t}+\sum_{t=1}^{T}\sum_{n=1}^{N}\sum_{k=1}^{K}E^{bc}_{n,t,k}+\sum_{t=1}^{T}\sum_{n=1}^{N}E^{z}_{n,t}\le\xi^*_I \quad (a)
\end{cases}
\tag{25}
$$

The lower bound (LB($h$)) is updated to max $\left\{\ LB(h),\ \xi^*_{II}-\sum_{t=1}^{T}\sum_{n=1}^{N}\beta^{g}_{n,t}\cdot P^{g,*}_{n,t}\cdot\Delta t\ \right\}$. Then, $\left(x^{v,h+1}_{j,t,b}, y^{v,h+1}_{j,t,b}, z^{v,h+1}_{j,t,b}\right)$ equals $\left(x^{v,*}_{j,t,k}, y^{v,*}_{j,t,k}, z^{v,*}_{j,t,k}\right)$. Variables $\left(E^{bc,h+1}_{n,t,k}, \mu^{h+1}_{n,t,1}, \mu^{h+1}_{n,t,2}, \mu^{h+1}_{n,t,3}, \mu^{l+1}_{n,t,4}, \mu^{h+1}_{n,t,5}\right)$ and constraints (23a)–(23i) are generated, and they are added to the MP. As a result, the first stage can be handled precisely and effectively by a commercial solver [52]. Then, the results $P^{g,first*}_{n,t}$ and $P^{unPV,first*}_{n,t}$ are sent to the second stage. Meanwhile, $P^{unPV,first*}_{n,t}$ is defined as $\max\left\{0,\ P^{PV}_{n,t}-\omega^{+}\cdot\sum_{b\in B^{n}_{BEV}}y^{v,first*}_{j^{n}_{ESA},t,b}\right\}$.

### 4.4. MEST scheduling in the second stage

In this section, the formulation of the spatial–temporal model for MESTs depicts the coupling relationship between charging and discharging of BESD and MESTs' spatial–temporal locations. Subsequently, leveraging the optimization results in the first stage and PV generation at SPESPs, the second stage schedules MESTs to alleviate the imbalance between energy supply and demand on expressways.

#### 4.4.1. Formulation of spatial–temporal network model for mobile energy storage trucks

This study introduces five binary variables and one continuous variable for MESTs to illustrate their dispatching and energy exchange on expressways. The binary variable $x^{er}_{j,t,m}$ indicates whether MEST $m$ in the right expressway lane passes through ES $j$ in time slot $t$, whereas $x^{el}_{j,t,m}$ indicates whether MEST $m$ in the left expressway lane passes through ES $j$. In time slot $t$, binary variables $y^{ech}_{j,t,m}$ and $y^{edis}_{j,t,m}$ indicate whether MEST $m$ charges or discharges in ESA $j$. The binary variable $z^{e}_{j,t,m}$ indicates whether MEST $m$ stays in ESA $j$ during the uncharged and undischarged periods. Eq. (26) defines MEST $m$ being situated in ESA $n$ during the first time slot. Eqs. (27)–(28) define the state shift between two neighboring ES spatial–temporal meshes for MESTs. This state shift in Eqs. (27)–(28) prevents MESTs from passing through ESAs and SPESPs, thereby denoting $j\ :\ \left\{j\in J^{Set}|j\notin J^{Set}_{ESA}\cup J^{Set}_{SPESP}\right\}$. Eqs. (29)–(30) ensure that MESTs are not allowed to exit expressways. Eq. (31) explains how MESTs shift their states as they move through ESAs between ESA 1 and ESA $N$. Therefore, $j\ :\ \left\{j\in J_{MEST}|j\neq j^{1}_{ESA},\ j\neq j^{N}_{ESA}\right\}$ is denoted in Eq. (31). Moreover, Eq. (32) defines how MESTs shift their states as they move through SPESPs. In the model, MESTs are assumed to only enter SPESPs when they move in the left lane. The unique state in every time slot for MESTs is guaranteed by Eq. (33). Eq. (34) guarantees every MEST being positioned in ESAs during the final time slot. Eqs. (35)–(36) restrict the energy exchange number for MESTs.

$$
y^{ech}_{j^{n}_{ESA},0,m}+y^{edis}_{j^{n}_{ESA},0,m}+z^{e}_{j^{n}_{ESA},0,m}=1\quad\forall n\in N^{Set},\ m\in M^{n}_{MEST} \tag{26}
$$

$$
x^{er}_{j-1,t-1,m}=x^{er}_{j,t,m}\quad\forall t\in T^{Set},\ m\in M^{Set} \tag{27}
$$

$$
x^{el}_{j,t-1,m}=x^{el}_{j-1,t,m}\quad\forall t\in T^{Set},\ m\in M^{Set} \tag{28}
$$

$$
\begin{aligned}
&x^{el}_{j^{1}_{ESA},t-1,m}+y^{ech}_{j^{1}_{ESA},t-1,m}+y^{edis}_{j^{1}_{ESA},t-1,m}+z^{e}_{j^{1}_{ESA},t-1,m}\\
&\quad=x^{el}_{j^{1}_{ESA},t,m}+y^{ech}_{j^{1}_{ESA},t,m}+y^{edis}_{j^{1}_{ESA},t,m}+z^{e}_{j^{1}_{ESA},t,m}\\
&\quad\forall t\in T^{Set},\ m\in M^{Set}
\end{aligned}
\tag{29}
$$

$$
x^{er}_{j^{N}_{ESA}-1,t-1,m}+y^{ech}_{j^{N}_{ESA},t-1,m}+y^{edis}_{j^{N}_{ESA},t-1,m}+z^{e}_{j^{N}_{ESA},t-1,m}
$$

$$= x^{el}_{j^N_{ESA}-1,t,m} + y^{ech}_{j^N_{ESA},t,m} + y^{edis}_{j^N_{ESA},t,m} + z^{e}_{j^N_{ESA},t,m}$$
$$\forall t \in T^{Set},\ m \in M^{Set} \tag{30}$$

$$x^{er}_{j-1,t-1,m} + x^{el}_{j,t-1,m} + y^{ech}_{j,t-1,m} + y^{edis}_{j,t-1,m} + z^{e}_{j,t-1,m} = x^{er}_{j,t,m} + x^{el}_{j-1,t,m} + y^{ech}_{j,t,m} + y^{edis}_{j,t,m} + z^{e}_{j,t,m}$$
$$\forall t \in T^{Set},\ m \in M^{Set} \tag{31}$$

$$x^{el}_{j,t-1,m} + y^{ech}_{j,t-1,m} + z^{e}_{j,t-1,m} = x^{el}_{j-1,t,m} + y^{ech}_{j,t,m} + +z^{e}_{j,t,m}$$
$$\forall t \in T^{Set},\ m \in M^{Set},\ j \in J^{Set}_{SPESP} \tag{32}$$

$$\sum_{j\in J_{MEST}} x^{er}_{j,t,m} + \sum_{j\in J_{MEST}} x^{el}_{j,t,m} + \sum_{j\in J^{Set}_{ESA}\cup J^{Set}_{SPESP}} y^{ech}_{j,t,m} + \sum_{j\in J^{Set}_{ESA}\cup J^{Set}_{SPESP}} y^{edis}_{j,t,m} + \sum_{j\in J^{Set}_{ESA}\cup J^{Set}_{SPESP}} z^{e}_{j,t,m} = 1$$
$$\forall t \in T^{Set},\ m \in M^{Set} \tag{33}$$

$$\sum_{m\in M^{Set}} (y^{ech}_{j^n_{ESA},T,m} + y^{edis}_{j^n_{ESA},T,m} + z^{e}_{j^n_{ESA},T,m}) = \alpha^{e}_{n} \quad \forall n \in N^{Set},\ m \in M^{Set} \tag{34}$$

$$\sum_{t\in T^{Set}} \sum_{j\in J^{Set}_{ESA}\cup J^{Set}_{SPESP}} y^{ech}_{j,t,m} \le \alpha^{lim}_{ech} \quad \forall m \in M^{Set} \tag{35}$$

$$\sum_{t\in T^{Set}} \sum_{j\in J^{Set}_{ESA}} y^{edis}_{j,t,m} \le \alpha^{lim}_{edis} \quad \forall m \in M^{Set} \tag{36}$$

The continuous variable $SOC^{e}_{t,m}$ represents the SOC of the BESD for MESTs. $E^{max}_{MEST}$ indicates the maximum BESD volume for MESTs. Eq. (37) defines the starting SOC for MESTs. Eq. (38) determines the SOC change of the BESD for MESTs in every time slot. $p^{ech}_{j,t,m}$ represents charging power for MEST $m$ in ESA $j$ or at SPESP $j$. $p^{edis}_{j,t,m}$ represents discharging power for MEST $m$ in ESA $j$. Eqs. (39)–(40) restrict the maximum charging and discharging power of the BESD for MESTs. Eq. (41) restricts the minimum SOC for MESTs.

$$SOC^{e}_{0,m} = \frac{E^{e}_{m}}{E^{max}_{MEST}} \quad \forall m \in M^{Set} \tag{37}$$

$$SOC^{e}_{t,m} \cdot E^{max}_{MEST} = SOC^{e}_{t-1,m} \cdot E^{max}_{MEST} + \Delta t \cdot \sum_{j\in J^{Set}_{ESA}} p^{ech}_{j,t,m} + \Delta t \cdot \sum_{j\in J^{Set}_{SPESP}} p^{ech}_{j,t,m} - \Delta t \cdot \sum_{j\in J^{Set}_{ESA}} p^{edis}_{j,t,m}$$
$$\forall t \in T^{Set},\ m \in M^{Set} \tag{38}$$

$$0 \le p^{edis}_{j,t,m} \le P^{max}_{edis} \cdot y^{edis}_{j,t,m} \quad \forall t \in T^{Set},\ m \in M^{Set},\ j \in J^{Set}_{ESA} \tag{39}$$

$$0 \le p^{ech}_{j,t,m} \le P^{max}_{ech} \cdot y^{ech}_{j,t,m} \quad \forall t \in T^{Set},\ m \in M^{Set},\ j \in J^{Set}_{ESA} \cup J^{Set}_{SPESP} \tag{40}$$

$$SOC^{min}_{MEST} \le SOC^{e}_{t,m} \quad \forall t \in T^{Set},\ m \in M^{Set} \tag{41}$$

#### 4.4.2. Objective function and power constraints

To optimize the scheduling of MESTs and maximize benefits, the objective function is defined in Eq. (42) and power constraints in Eqs. (47)–(49) in the second stage. This framework aims to allocate surplus PV generation, not utilized for BEV charging, to grid-supplying BEV loads. $E^{edis}_{m}$, $U^{ep}_{m}$, $U^{ech}_{m}$, and $U^{edis}_{m}$ in Eq. (42) are the auxiliary variables. They are continuous variables, and the detailed expressions for them are illustrated in Eqs. (43)–(46). In detail, $E^{edis}_{m}$ indicates the income of the expressway manager scheduling MESTs to supply the BEV loads that PV generation cannot satisfy. This income is derived from using the energy generated by PV installations stored in MESTs to replace the grid and supply BEV charging. $U^{ep}_{m}$ denotes the moving expense for MESTs on expressways, whereas $U^{ech}_{m}$ and $U^{edis}_{m}$ represent the charging and discharging degradation expenses of BESD for every MEST. In ESA $n$, Eq. (47) indicates surplus PV generation is used to charge BESDs installed in MESTs, while Eq. (49) represents that BESDs provide energy for grid-supplying charging demands. Eq. (48) indicates that PV generation at SPESP $a$ is used to charge BESDs. Eq. (50) ensures that MESTs cannot transmit energy to each other.

$$\max \sum_{m=1}^{M} \left(E^{edis}_{m} - U^{ep}_{m} - U^{ech}_{m} - U^{edis}_{m}\right) \tag{42}$$

$s.t.$ (26)–(41)

$$E^{edis}_{m} = \sum_{n\in N^{Set}} \sum_{t\in T^{Set}} \beta^{g}_{n,t} \cdot \Delta t \cdot p^{edis}_{j^n_{ESA},t,m} \quad \forall m \in M^{Set} \tag{43}$$

$$U^{ep}_{m} = \sum_{j\in J_{MEST}} \sum_{t\in T^{Set}} v^{ep} \cdot \left(x^{er}_{j,t,m} + x^{el}_{j,t,m}\right) \quad \forall m \in M^{Set} \tag{44}$$

$$U^{ech}_{m} = \sum_{j\in J^{Set}_{SPESP}} \sum_{t\in T^{Set}} v^{ech} \cdot \Delta t \cdot p^{ech}_{j,t,m} + \sum_{j\in J^{Set}_{ESA}} \sum_{t\in T^{Set}} v^{ech} \cdot \Delta t \cdot p^{ech}_{j,t,m}$$
$$\forall m \in M^{Set} \tag{45}$$

$$U^{edis}_{m} = \sum_{j\in J^{Set}_{ESA}} \sum_{t\in T^{Set}} v^{ech} \cdot \Delta t \cdot p^{edis}_{j,t,m} \quad m \in M^{Set} \tag{46}$$

$$\sum_{m=1}^{M} p^{ech}_{j^n_{ESA},t,m} \le P^{unPV,first*}_{n,t} \quad \forall n \in N^{Set},\ t \in T^{Set} \tag{47}$$

$$\sum_{m=1}^{M} p^{ech}_{j^a_{SPESP},t,m} \le P^{PV}_{a,t} \quad \forall a \in A^{Set},\ t \in T^{Set} \tag{48}$$

$$\sum_{m=1}^{M} p^{edis}_{j^n_{ESA},t,m} \le P^{g,first*}_{n,t} \quad \forall n \in N^{Set},\ t \in T^{Set} \tag{49}$$

$$\sum_{m=1}^{M} p^{ech}_{j^n_{ESA},t,m} \le M \cdot \left(1 - p^{edis}_{j^n_{ESA},t,m}\right) \quad \forall n \in N^{Set},\ t \in T^{Set} \tag{50}$$

The MEST scheduling problem in the second stage is formulated as a MILP model, which can be directly solved by a commercial solver.

## 5. Case study

This section presents a case study to demonstrate the effectiveness of the proposed two-stage scheduling method.

### 5.1. Case description and basic settings

In this study, an expressway system based on the Lianhuo and Jingkun expressways in China is introduced for an experimental study. Fig. 5 shows that the system has two expressway entrances, five ESAs, one SPESP, and one exit. The map data presented in Fig. 5 is retrieved from Amap [53]. The expressway system consists of 12 ESs, each measuring 50 km, resulting in a total length of approximately 600 km. In this system, there are two blue rhombuses representing expressway entrances, Mianchi and Xi'an. The orange rhombus represents the only exit, which is Ningqiang. There are five ESAs represented by purple triangles, each containing an EVCS. Two ESAs are located approximately 100 km apart. Entrance Mianchi is located 100 km from ESA1, Entrance Xi'an is positioned 50 km from ESA3, and Exit Ningqiang is situated 100 km from ESA5. This study assumes that the system has only one SPESP. The red circle represents this SPESP, which is located between ESA1 and ESA2. The operational task from 0:00 a.m. to 7:00 a.m. is disregarded due to the lower BEV traffic volume during this time. Then, this study divides the operational horizon into 34 time slots, ranging from 7:00 a.m. to 12:00 p.m.

Fig. 6 shows PV generation profiles in each time slot in five ESAs and at the SPESP. The installed PV capacity in these areas is set at 0.6

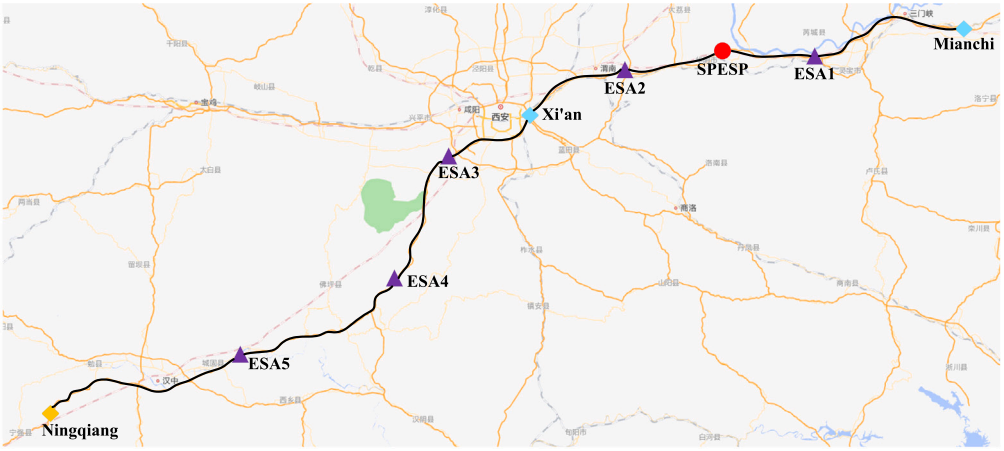


**Fig. 5.** Illustration of the expressway system.

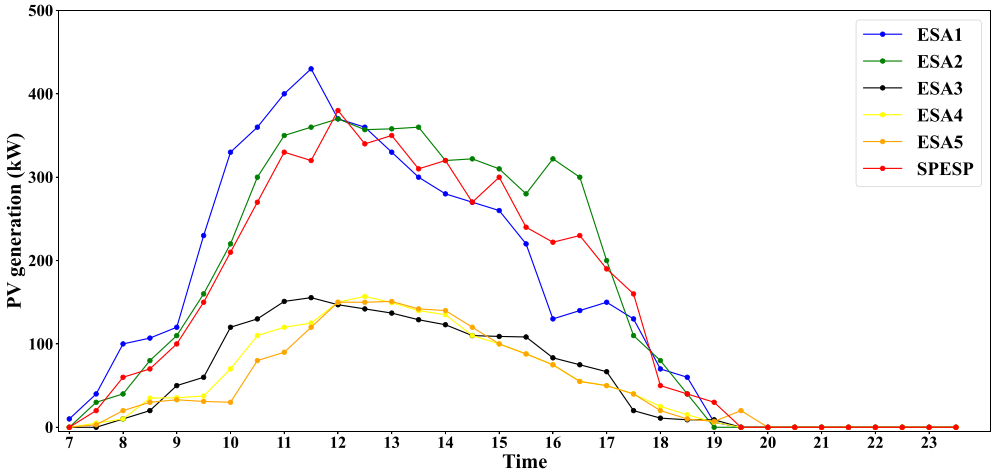


**Fig. 6.** PV generation along expressways.

MW. Spatial disparities in PV generation may occur due to variations in solar radiation or weather across regions, as a result of the geographic distribution of ESAs and SPESPs along expressways. Notably, segments of the expressway between ESA1 and ESA2 experience higher solar radiation levels, resulting in greater PV generation in these areas (ESA1, ESA2, and SPESP) compared to others.

The basic parameter settings for BEVs and MESTs are illustrated in Table 5. The parameters for MESTs are derived from the studies conducted by [54,55]. This study sets up six MESTs in the expressway system and assume they have the same parameter values. During the initial time slot, MESTs stay in ESAs 2–4. Meanwhile, MEST1 and MEST2 stay in ESA2. MEST3 and MEST4 stay in ESA3. MEST5 and MEST6 stay in ESA4. For BEVs, the parameters are modeled on the specifications of the BYD Han BEV [56]. The quantified time expenditure of BEV drivers during their uncharged period, denoted as $\beta^{vtime}$, is estimated based on the average hourly wage in China [57]. Parking fees for vehicles are typically charged on an hourly basis. This study also adopts this method. Additionally, parking fees for vehicles, including BEVs, are generally charged on an hourly basis [58], and this method has been adopted in this case study.

Figs. 7 and 8 illustrate the numbers of BEVs during every time slot at Entrances Mianchi and Xi'an. Xi'an City, Shanxi Province's capital, has a larger population density and number of companies than Mianchi County. As a result, the BEV's number at Entrance Xi'an exceeds that at Entrance Mianchi.

Referring to existing research [20,22,25,36,59], six comparative cases are designed to analyze the effectiveness of the proposed two-stage scheduling approach in improving PV generation utilization. The proposed two-stage scheduling approach is defined as a basic case. The details of the comparative cases are as follows:

(1) Comparative case 1: Existing research [25] did not incorporate the MEST scheduling method to enhance PV generation utilization. This case refers to the strategy from [25], focusing solely on BEV scheduling. The model and parameter values used are the same as those in the first stage of the basic case.
(2) Comparative case 2: This case employs a two-stage scheduling method. In the first stage, BEVs are scheduled using the same model as in the first stage of the basic case. In the second stage, MESTs are scheduled without considering PV generation and BEV charging loads [36], based on a fixed time-space table. In detail, MEST1 charges from 7:30 a.m. to 10:30 a.m. in ESA2 and discharges from 11:30 a.m. to 15:30 p.m. in ESA1; MEST2 charges from 8:30 a.m. to 14:00 p.m. at the SPESP and discharges from 15:30 p.m. to 19:30 p.m. in ESA1; MEST3 charges from 7:30 a.m. to 10:30 a.m. and discharges from 15:30 p.m. to 18:30 p.m. in ESA3; MEST4 charges from 10:30 a.m. to 13:00 p.m. in ESA3 and discharges from 15:30 p.m. to 18:30 p.m. in ESA2; MEST5 charges from 7:30 a.m. to 10:30 a.m. in ESA4 and discharges from 12:30 p.m. to 15:30 p.m. in ESA5; MEST6 charges from 9:30 a.m. to 13:30 p.m. and discharges from 15:30 p.m. to 19:30 p.m. in ESA5.

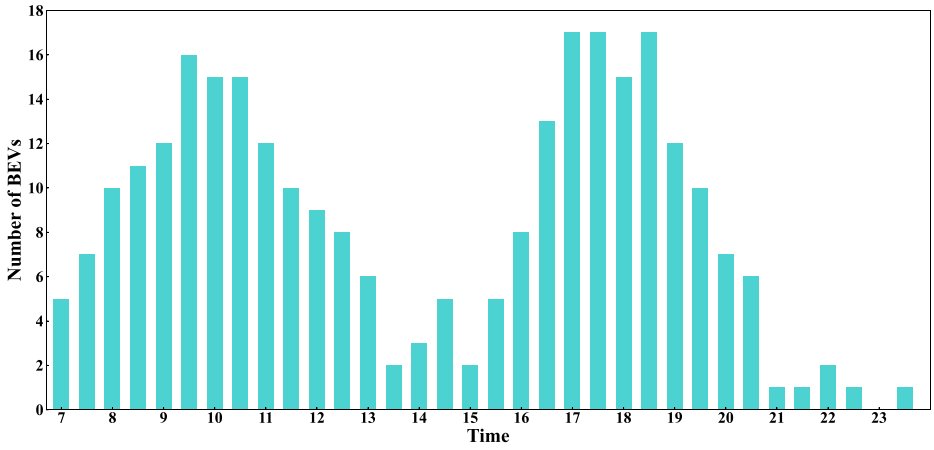


**Fig. 7.** Number of BEVs entering expressways at Entrance Xi'an.

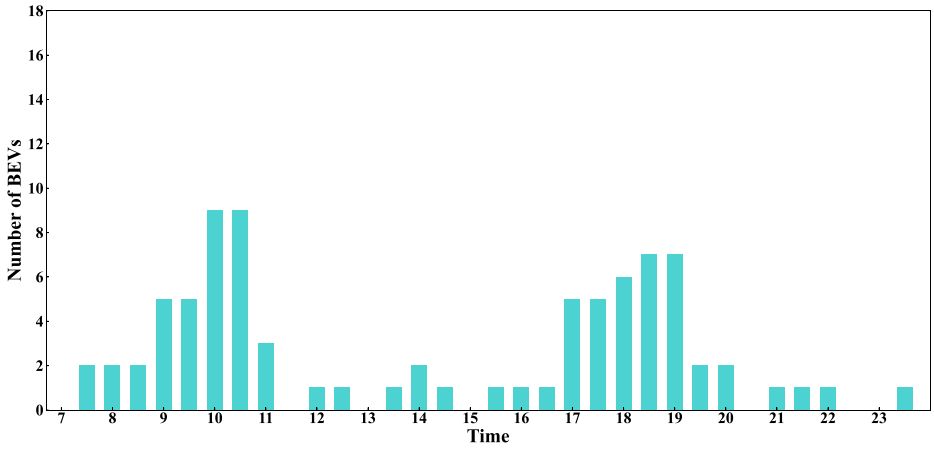


**Fig. 8.** Number of BEVs entering expressways at Entrance Mianchi.

**Table 5**
Basic parameter settings for MESTs and BEVs.

| Parameters | Values |
|---|---|
| Moving speed for BEVs and MESTs | 100 km/h |
| Battery volume for every BEV | 75 kWh |
| Electric consumption rate of battery per kilometer for every BEV | 0.15 kWh/km |
| Initial battery level for every BEV at Entrance Xi'an | 37.5 kWh |
| Initial battery level for every BEV at Entrance Mianchi | 60 kWh |
| Minimum SOC for every BEV | 0.1 |
| Charging power for every BEV at every EVCS in ESA | 30 kW/h |
| Optional charging prices at every EVCS | 1.5/2/2.5/3 RMB/kWh |
| BESD volume for every MEST | 1 MWh |
| Minimum SOC of BESD for every MEST | 0.1 |
| Maximum BESD charging power for every MEST | 120 kW |
| Discharging and charging degradation expenses of the BESD for every MEST | 0.21 RMB/kWh |
| Maximum BESD discharging power for every MEST | 500 kW |
| Moving expense per ES for every MEST | 3 RMB |
| BEV charging load limit for the EVCS in every ESA | 700 kW |
| Temporal cost of BEV parking indicating the quantified time expenditure of BEV drivers during their uncharged period | 22 RMB/h |
| Parking fees for BEVs in ESAs in one time slot (uncharged period) | 1.1 RMB/h |

(3) Comparative case 3: In research [20,22], PV generation and LMP are not considered in BEV scheduling. Referring to this strategy, this case formulates the BEV charging schemes according to the time-of-use charging price to minimize charging costs.

(4) Comparative case 4: This case adopts a two-stage scheduling method. To minimize charging costs, BEV charging plans are developed in the first stage based on the time-of-use charging price. Then, MESTs are scheduled in the second stage using the

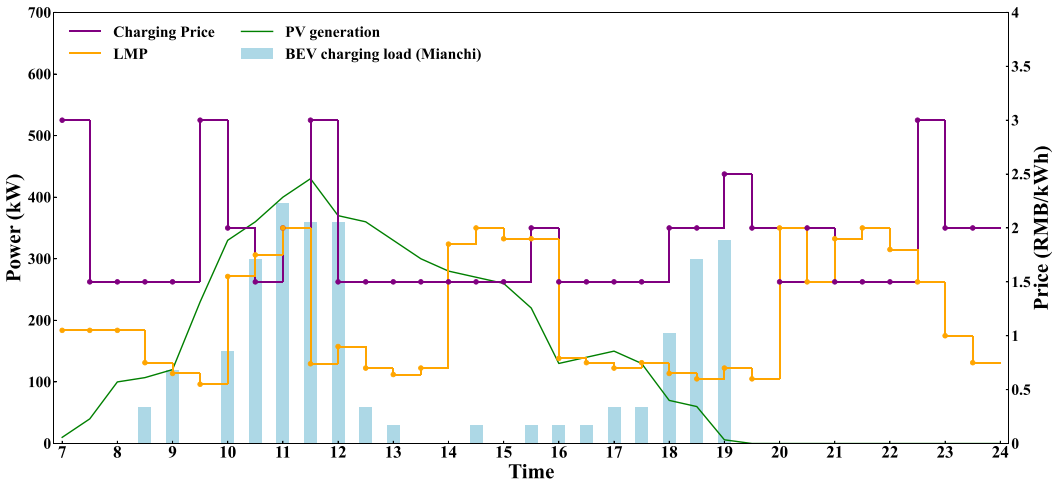


**Fig. 9.** BEV charging loads, LMP, charging prices, and PV generation profiles in ESA1.

same model and parameter values as the second stage of the basic case.

(5) Comparative case 5: This case examines the LMP across various ESAs and formulates BEV charging schemes aimed at maximizing profits for the expressway manager [59]. In contrast to Eq. (17) in the basic case model, the power constraint for basic BEV charging in this comparative case considers only the energy supplied from the grid, as shown in Eq. (51). The parameters and other components of the model used in the comparative case are the same as those in the first stage of the basic case.

$$P^{g}_{n,t} \geq \omega^{+} \cdot \sum_{b \in B^{n}_{BEV}} y^{v}_{j^{n}_{ESA},t,b} \quad \forall n \in N^{Set},\ t \in T^{Set} \tag{51}$$

(6) Comparative case 6: This case adopts a two-stage scheduling method. The first-stage model follows the same approach as in the comparative case 5, which considers LMP in different ESAs. In the second stage, MESTs are scheduled using the same model and parameter values as those in the second stage of the basic case.

Next, this study implements the mathematical model in Python 3.8 and solves it using Gurobi 11 [60].

### 5.2. Results and discussions of battery electric vehicle charging scheduling

In the first stage, the optimal solutions for BEV charging scheduling are obtained. This section will show and discuss the results.

#### 5.2.1. Spatial–temporal distributions of battery electric vehicle charging load

The spatial–temporal distributions of BEV charging loads are presented in Figs. 9–13. The charging loads of BEVs entering the expressway at Entrances Mianchi and Xi'an are represented by light blue and gray colored bars. Figs. 9–13 also comprise LMP, PV generation, and BEV charging prices in every ESA. Initially, the concentration of BEV charging loads in the first stage is scheduled during rich PV-generating time slots. For instance, BEV charging loads in Fig. 9 are concentrated from 10:30 a.m. to 12:30 p.m. in ESA1. Fig. 10 shows BEV charging loads are concentrated from 12:30 p.m. to 13:30 p.m. in ESA2. Similarly, Fig. 11 shows BEV charging loads in ESA3 are concentrated at 13:30 p.m.–14:30 p.m., whereas BEV charging loads in Fig. 13 are concentrated from 11:00 a.m.–12:30 p.m. in ESA5. This approach allows for a moderate increase in PV generation consumption.

During the specified time slots, PV power generation is sufficient to meet the demands of charging BEVs. However, in cases where PV generation alone is not enough, both the LMP and PV generation work together to influence BEV charging loads. For instance, Figs. 11–12 show the schedules for BEV charging loads in ESA3 and ESA4, with their concentrations scheduled at 11:00 a.m.–13:30 p.m. and 10:30 a.m.–11:30 a.m., respectively. Due to the higher charging demands in ESA3 and ESA4, meeting these demands solely through PV generation is challenging. During richer PV-generating periods, the concentration of the above unsatisfied charging demands in lower LMP time slots can further decrease the expressway manager's purchasing electricity cost. Moreover, the charging loads generated by BEVs entering expressways after rich PV-generating periods are only impacted by LMP. For example, Figs. 10–11 show peak BEV charging loads in ESA2 and ESA3, with concentrations between 20:00 p.m. and 21:30 p.m.. The BEV charging loads in Fig. 13 are scheduled to be concentrated in ESA5 between 20:00 p.m.–21:00 p.m.

The above results highlight that scheduling BEV to charge during rich PV-generating periods significantly enhances PV generation utilization while reducing reliance on the grid. In cases where PV generation is insufficient, the integration of LMP effectively balances the energy demand, optimizing electricity costs for the expressway manager. This plan not only improves solar energy consumption but also minimizes operational costs, demonstrating the efficiency of the proposed first-stage approach in managing BEV charging loads in ESAs.

Under the proposed first-stage method, most charging-load concentration periods do not set high charging prices. For example, lower charging prices in Fig. 9 are set at 10:30 a.m.–11:30 a.m. in ESA1. Lower charging prices in Fig. 11 are set from 11:30 a.m. to 12:30 p.m. in ESA3. Lower charging prices in Fig. 12 are set from 10:00 a.m. to 11:30 a.m. in ESA4. In practice, the expressway manager's charging schemes tend to attract more BEV drivers due to their lower charging costs.

#### 5.2.2. Convergence of the proposed first-stage method

This section demonstrates the convergence of the proposed first-stage method based on the C&CG approach. Fig. 14 depicts $\frac{\mathrm{UB}(h)-\mathrm{LB}(h)}{\mathrm{LB}(h)}$ calculated at every iteration. Algorithm 1 converges when $\mu$ is greater than or equal to $\frac{\mathrm{UB}(h)-\mathrm{LB}(h)}{\mathrm{LB}(h)}$, where $\mu$ is equal to 0.115. The proposed first-stage method converges after 11 iterations, and the calculation time is approximately 120 min, which is acceptable for day-ahead scheduling.

The upper bound (UB) and lower bound (LB) values at certain iterations (0, 3, 8, 10) are shown in Table 6. The UB value decreases from 25 575.8 to 14 576.7, which further illustrates that our first-stage method considers the BEV drivers' benefit.

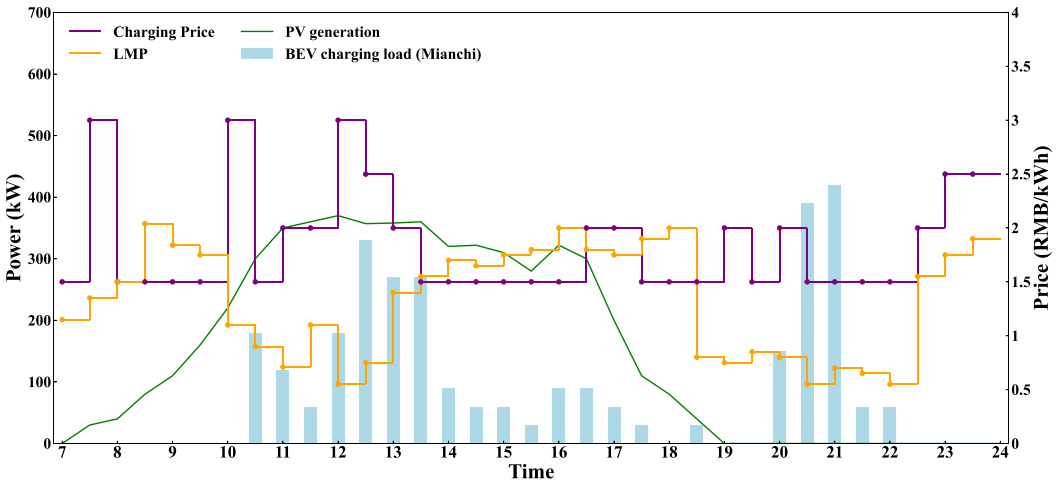


**Fig. 10.** BEV charging loads, LMP, charging prices, and PV generation profiles in ESA2.

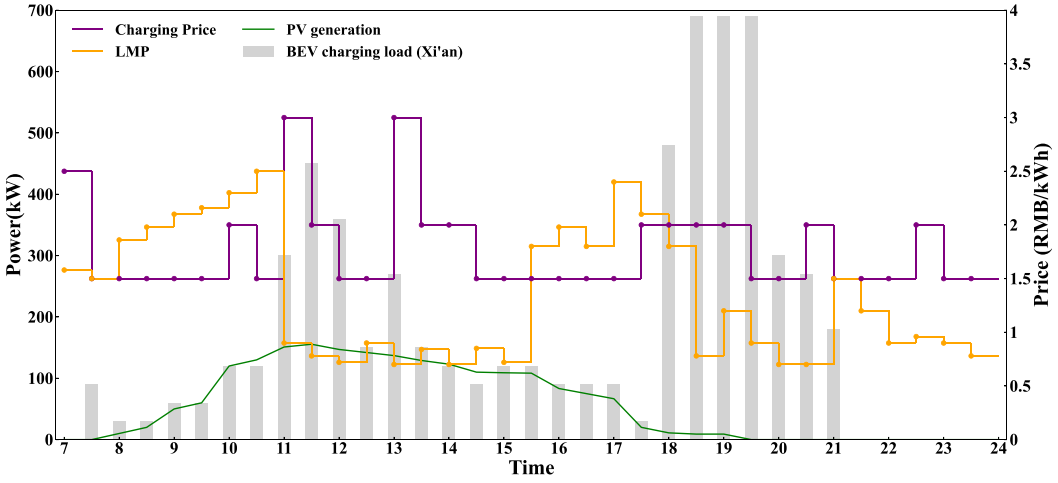


**Fig. 11.** BEV charging loads, LMP, charging prices, and PV generation profiles in ESA3.

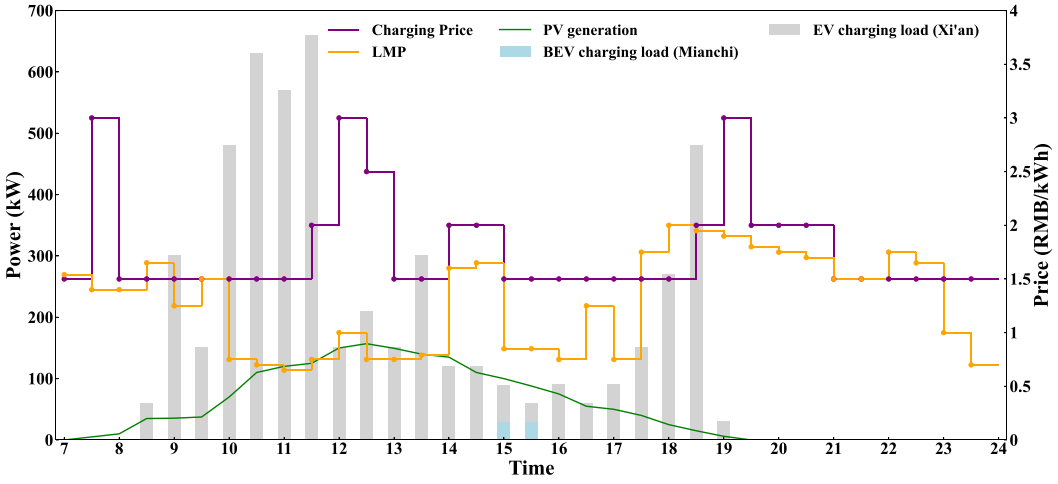


**Fig. 12.** BEV charging loads, LMP, charging prices, and PV generation profiles in ESA4.

### 5.2.3. PV generation supply and BEV charging demand

Fig. 15 illustrates the total PV generation supply and BEV charging demand in ESAs and at the SPESP. Firstly, the proposed method effectively depicts the unidirectionality of BEVs on expressways, as no charging demands from Entrance Xi'an are distributed in ESA1 and ESA2. Secondly, no BEVs are assigned to charge at the SPESP, adhering to the limit that prohibits BEVs from charging there. Thirdly, ESAs 3–5 exhibit higher charging demands compared to ESA1, ESA2, and SPESP, which have more abundant PV generation. According to Figs. 5 and 7, a large number of BEVs enter expressways at Entrance Xi'an and

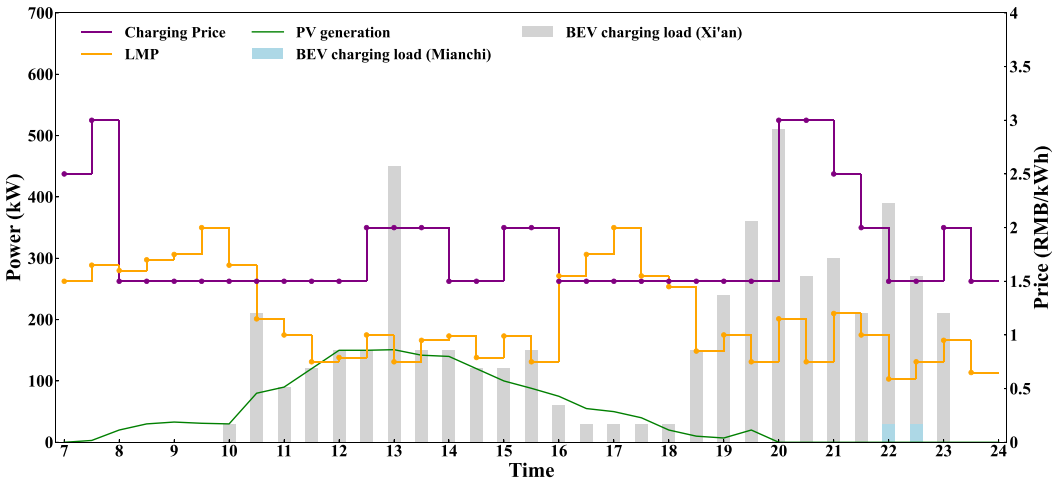


**Fig. 13.** BEV charging loads, LMP, charging prices, and PV generation profiles in ESA5.

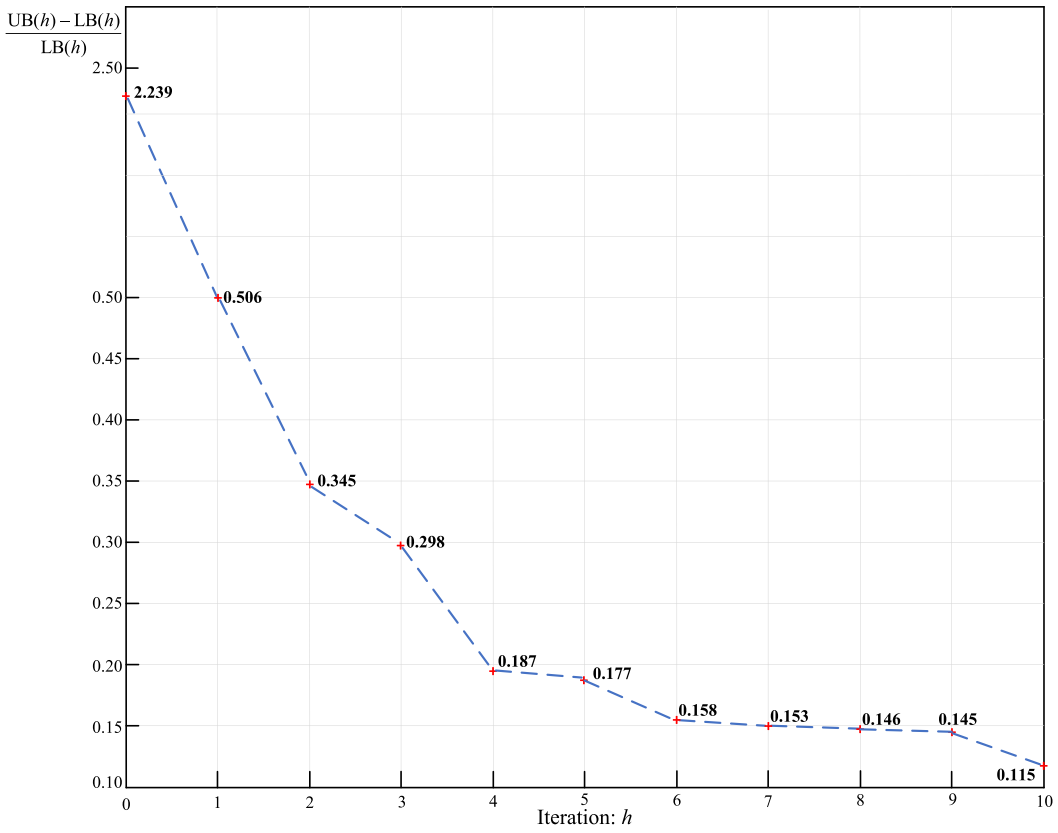


**Fig. 14.** Convergence of the proposed first-stage method.

**Table 6**
The UB and LB values at certain iterations.

| Bound | Iteration 0 | Iteration 3 | Iteration 8 | Iteration 10 |
|---|---|---|---|---|
| UB (RMB) | 25 575.8 | 15 087.4 | 14 611.5 | 14 576.7 |
| LB (RMB) | 7895.2 | 11 619.4 | 12 745.1 | 13 066.0 |

drive to Ningqiang, resulting in higher charging demands in ESAs 3–5. Due to the unidirectionality of BEVs on expressways, the expressway manager is unable to schedule BEVs accessing expressways at Entrance Xi'an to charge in ESA1 and ESA2 with richer PV generation. Moreover, BEVs cannot charge at SPESP to consume PV generation. As a result, addressing the spatial supply–demand imbalance proves to be challenging through the first stage of reshaping BEV charging loads. In ESAs 3–5, BEV charging demands exceeding PV generation must be supplied by the grid.

### 5.3. Results and discussion of mobile energy storage truck scheduling

In the second stage, the optimal solutions for MEST scheduling are obtained. This section will show and discuss the results.

#### 5.3.1. Spatial–temporal state shifts for mobile energy storage trucks

Fig. 16 presents the spatial–temporal state shifts for six MESTs. The SOC results for every MEST are calculated as BESD levels to illustrate the energy change in each state, as shown in the upper part of each

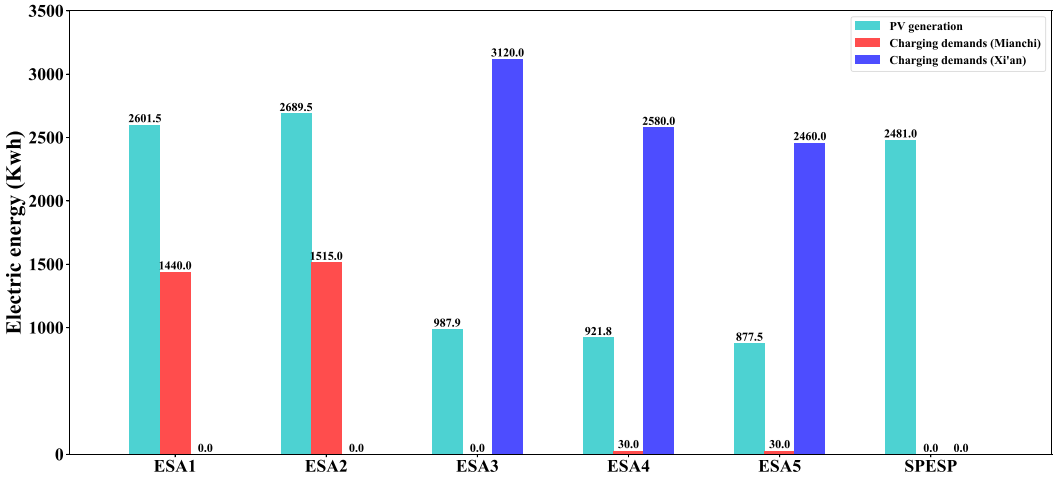


**Fig. 15.** Diagram of PV generation supply and BEV charging demand.

subfigure. In accordance with Section 5.2.3, ESA1, ESA2, and the SPESP have additional PV generation that has not been used. Therefore, MEST is dispatched to these areas to supplement the BESD. Specifically, in Fig. 16(a), MEST1 moves to ESA1 to charge its BESD based on unconsumed PV generation. After charging its BESD to 635 kWh, it performs a U-turn in ESA1's steering corridor and returns to ESA2 to continue the remaining charging tasks to 755 kWh. Similarly, based on unconsumed PV generation, the study suggests that MEST3 should charge its BESD to 635 kWh at ESA2, MEST4 should charge to 744 kWh at ESA2, and MEST5 should charge to 760 kWh at the SPESP. These are shown in Figs. 16(c), 16(d), and 16(e), respectively. The difference is that MEST2 and MEST6 require two charging sessions. Specifically, MEST2 in Fig. 16(b) first charges to 567 kWh at SPESP, and it charges to 747 kWh in ESA1. MEST6 in Fig. 16(f) first charges to 753 kWh at SPESP, and it charges to 813 kWh in ESA2. The implementation allows MESTs 1–6 to dynamically adjust charging locations based on PV generation, thereby maximizing efficiency and completing PV generation storage.

In terms of optimizing the schedule of MESTs, this study finds that the optimal strategy is to schedule MEST1 to ESA3, MEST4 to ESA5, and MEST6 to ESA5, each with a BESD discharge of 644 kWh, 644 kWh, and 713 kWh, respectively. Furthermore, MEST2 and MEST3 must complete two scheduling actions: MEST2 to ESA4 and ESA3, and MEST3 to ESA3 and ESA5, with BESD discharges of a total of 647 and 568.5 kWh, respectively. Moreover, MEST5 supplies 660 kWh of BESD to ESA1 and ESA2 to charge BEVs entering expressways after high PV-generating periods in these ESAs. The aforementioned findings demonstrate the effectiveness of MESTs in the space transfer of PV generation.

Each MEST's BESD level can comply with SOC constraints in every time slot. That is, BESD levels for all MESTs vary between 0.1 and 1 MWh. According to calculations, total charging and discharging energies for all MESTs are equivalent, indicating that the proposed second-stage method considers the degradation expenses of the BESD.

In summary, by aligning MEST deployments with spatial–temporal PV generation and charging demands, the strategy reduces clean energy waste and improves the utilization of solar resources. Additionally, the compliance with SOC constraints and consideration of BESD degradation expenses highlight the efficiency and practicality of the proposed second-stage method.

### *5.3.2. Spatial–temporal distributions of charging/ discharging power for mobile energy storage trucks*

Figs. 17–22 show the detailed spatial–temporal distributions of charging and discharging power for MESTs in every ESA. The light gray bars depict the BEV charging loads supplied by the grid in the first stage, indicating that these charging loads surpass the PV generation in these specific time-space locations. Since BEVs are prohibited from charging at the SPESP, Fig. 22 excludes MEST discharging power and charging loads supplied by the grid.

The proposed second-stage method schedules MEST charging power to concentrate in time-space locations with more unconsumed PV generation. For instance, MEST1 and MEST2 in Fig. 17 are scheduled to charge their BESDs from 13:00 p.m. to 14:30 p.m. in ESA1, while MEST3 and MEST4 in Fig. 18 are scheduled to charge their BESDs at 11:00 a.m.–12:30 p.m. and 14:00 p.m.–15:30 p.m. in ESA2. In Fig. 22, MEST2, MEST5, and MEST6 are scheduled to charge their BESDs from 12:00 p.m. to 12:30 p.m. at the SPESP. MEST2 and MEST5 are scheduled to charge their BESDs from 10:00 a.m. to 11:30 a.m. at the SPESP. MEST5 and MEST6 are scheduled to charge their BESDs from 12:30 p.m. to 15:30 p.m. at the SPESP. This allows MESTs to store more unconsumed PV generation in their BESDs.

Moreover, MEST discharging power is mainly scheduled in time-space locations with grid-supplying charging loads. For instance, MEST5 in Fig. 17 is scheduled to supply charging loads supplied by the grid from 18:00 p.m. to 19:30 p.m. in ESA1. MEST1 and MEST6 in Fig. 19 are scheduled to supply charging loads supplied by the grid from 18:30 p.m. to 20:30 p.m. in ESA3. MEST4 in Fig. 21 is scheduled to supply charging loads supplied by the grid at 18:30 p.m.–20:30 p.m. in ESA5. MEST3 in Fig. 21 is scheduled to supply charging loads supplied by the grid from 20:30 p.m. to 22:30 p.m. in ESA5. The above time-space locations have the characteristic of a concentrated distribution. MESTs discharging in these time-space locations can reduce dispatching expenses while transmitting more energy to BEVs. Furthermore, the LMP also impacts the distribution of MEST discharging. For instance, MEST3 in Fig. 19 is scheduled to supply charging loads supplied by the grid from 17:00 p.m. to 18:00 p.m. in ESA3. MEST2 in Fig. 20 is scheduled to supply charging loads supplied by the grid at 18:30 p.m.–19:30 p.m. in ESA4. In the above situation, MESTs are scheduled to discharge when the LMP is higher, which results in consuming PV generation and reducing purchasing electricity expenses.

Overall, the proposed second-stage method effectively schedules MESTs to manage their charging and discharging actions on expressways, synchronizing them with unconsumed PV generation and grid-supplying charging loads. By concentrating MEST charging during rich PV-generating periods and discharging during high LMP intervals, the approach minimizes grid dependency and lowers electricity costs. This adjustment of spatial–temporal energy distribution enhances PV generation utilization while satisfying charging demands and optimizing operational costs.

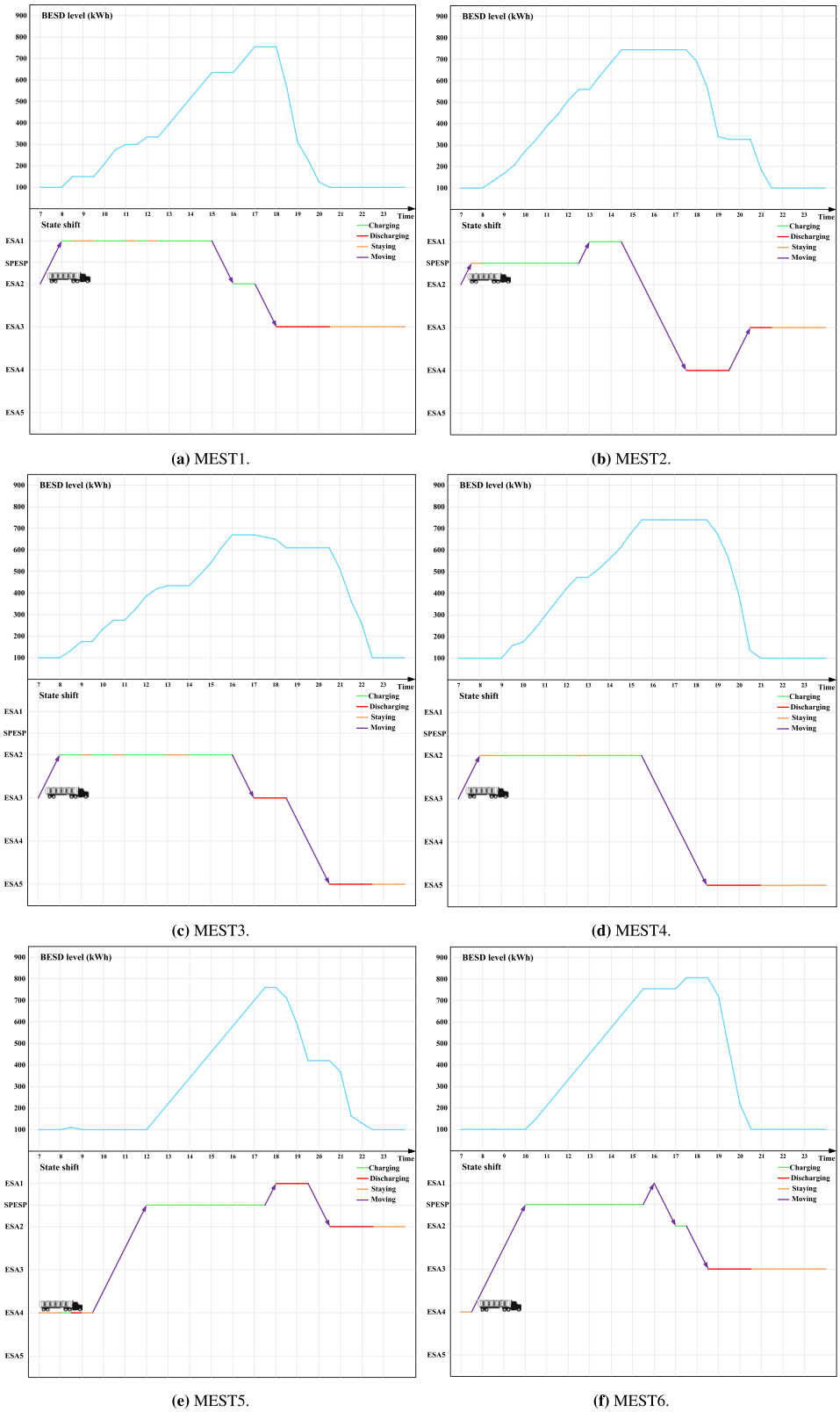


(**a**) MEST1. (**b**) MEST2.

(**c**) MEST3. (**d**) MEST4.

(**e**) MEST5. (**f**) MEST6.

**Fig. 16.** Spatial–temporal state shifts and BESD level for six MESTs.

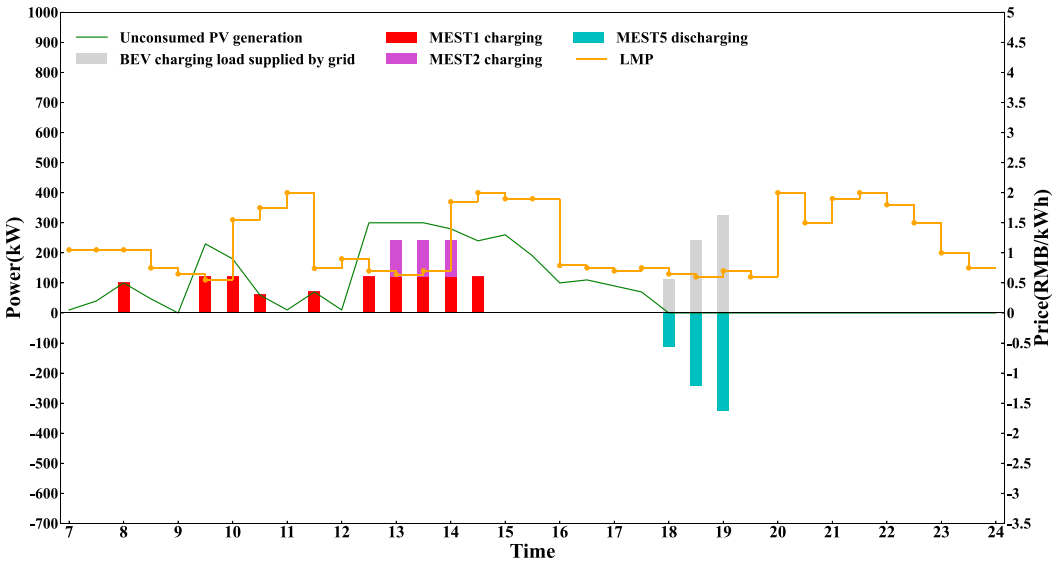


**Fig. 17.** MEST charging and discharging power, LMP, and unconsumed PV generation profiles in ESA1.

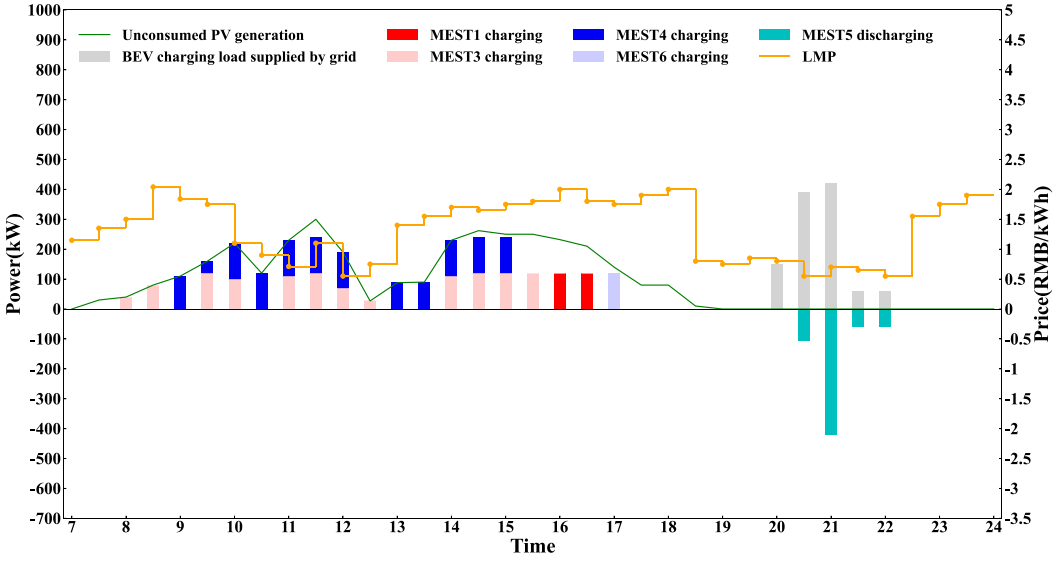


**Fig. 18.** MEST charging and discharging power, LMP, and unconsumed PV generation profiles in ESA2.

### *5.4. Photovoltaic generation utilization in the basic and comparative cases*

Fig. 23 shows that the basic case has the highest total PV generation utilization compared to the comparative cases 1–6, indicating the effectiveness of the proposed two-stage scheduling approach in the utilization of PV generation.

Specifically, the total PV generation utilization in the basic case has increased by 36.9% compared to the comparative case 1. This significant improvement is attributed to the expansion of ESA1, ESA2, and SPESP, especially at the SPESP where scheduling MESTs is the sole method for consuming PV generation, leading to a notable 71.8% surge. Fig. 16 demonstrates that the total charging energy equals the total discharging energy for every MEST. As a result, MESTs can efficiently use the PV-generating energies stored in BESDs, significantly increasing PV power utilization. Moreover, the total PV generation utilization in the basic case has grown by 33.4% compared to the comparative case 2. This suggests that the MEST scheduling approach, grounded in the energy supply–demand relationship, offers distinct advantages in increasing PV generation utilization over methods reliant on the spatial–temporal table.

In the comparative case 2, total PV generation utilization is 22.6% higher than in comparative case 3 and 18.8% higher than in the comparative case 5, highlighting the effectiveness of the proposed first-stage method, which integrates both PV generation and BEV drivers' benefits from the basic case. In contrast, the comparative case 3 formulates BEV charging plans solely to minimize drivers' costs, while the comparative case 5 considers LMP in charging schemes. Neither of these two cases accounts for PV generation on expressways. Additionally, the comparative case 4, which applies the second-stage method from the basic case with identical models and parameters, achieves a 35.7% increase in PV generation utilization compared to the comparative case 3. Similarly, the comparative case 6, also using the second-stage method from the basic case, demonstrates a 35.7% increase in PV generation utilization compared to the comparative case 5. These findings suggest that even when the first-stage method does not consider PV generation, the proposed second-stage method remains effective in enhancing PV generation utilization.

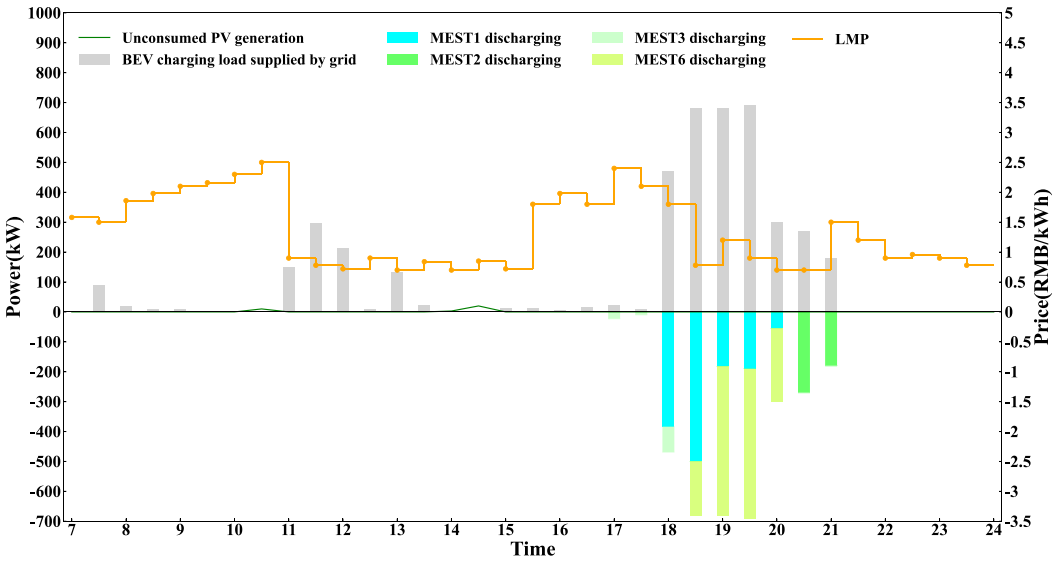


**Fig. 19.** MEST charging and discharging power, LMP, and unconsumed PV generation profiles in ESA3.

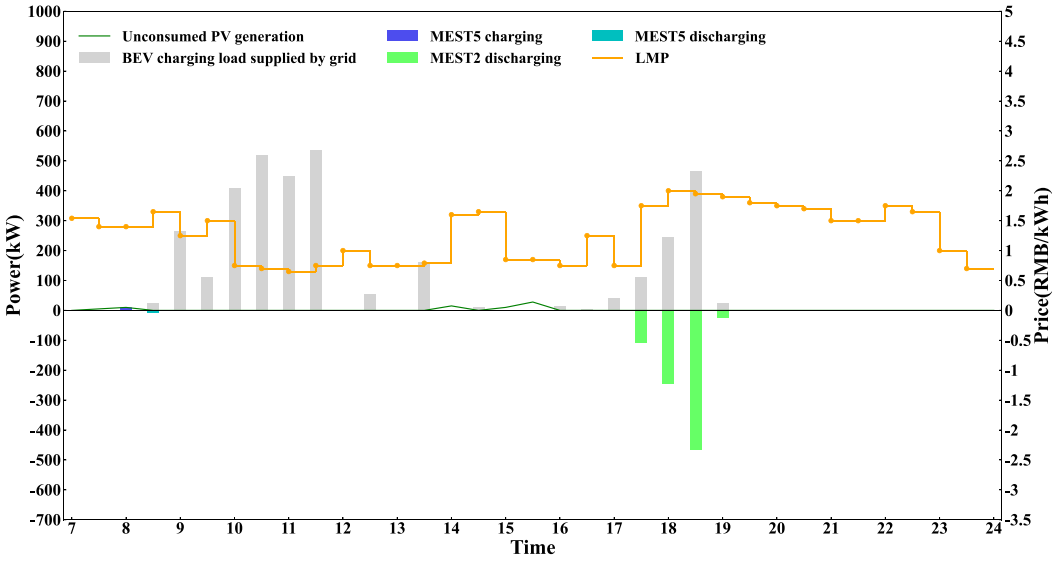


**Fig. 20.** MEST charging and discharging power, LMP, and unconsumed PV generation profiles in ESA4.

**Table 7**
Grid electricity purchase costs and carbon emission in the basics and comparative cases.

| Case | Grid electricity purchase costs | Carbon emissions |
|---|---|---|
| Basic case | 2122.0 RMB | 1536.8 kg |
| Comparative case 1 | 6230.5 RMB | 3872.3 kg |
| Comparative case 2 | 5983.1 RMB | 3653.3 kg |
| Comparative case 3 | 9815.3 RMB | 5292.4 kg |
| Comparative case 4 | 4271.9 RMB | 3025.3 kg |
| Comparative case 5 | 7540.8 RMB | 4722.2 kg |
| Comparative case 6 | 3196.5 RMB | 2460.5 kg |

Table 7 presents the grid electricity purchase costs and carbon emissions for both the basic and comparative cases. In this study, carbon emissions are estimated using an average electricity emission factor of approximately 0.6 kg/kWh in China [61]. Among all cases, the basic case incurs the lowest electricity purchase cost of 2122 RMB, highlighting the economic advantages of increased PV generation utilization for expressway management. Furthermore, the basic case also has the lowest carbon emissions (1536.8 kg) among the cases, demonstrating the effectiveness of the proposed two-stage scheduling method in reducing carbon emissions.

### 5.5. Scalability of the proposed two-stage scheduling method

To demonstrate the scalability of the proposed two-stage scheduling approach, this study designs an extended case. As illustrated in Fig. 24, the expressway system in the extended case comprises two expressway entrances, seven ESAs, one SPESP, and one exit. The system in the extended case consists of 16 ESs, each measuring 50 km, resulting in a total length of approximately 800 km. The locations of the two entrances (Xi'an and Mianchi) and the SPESP remain the same as in the basic case. Similar to the basic case, two ESAs are located approximately 100 km apart. Notably, the orange rhombus represents Exit Jiangyou, which is situated 100 km from ESA7 due to the increase in the length of the expressway system in the extended case.

In the extended case, twice as many BEVs enter expressways at Entrances Xi'an and Mianchi during every time slot as in the basic case. Hence, the number of BEVs in the extended case increases by 355

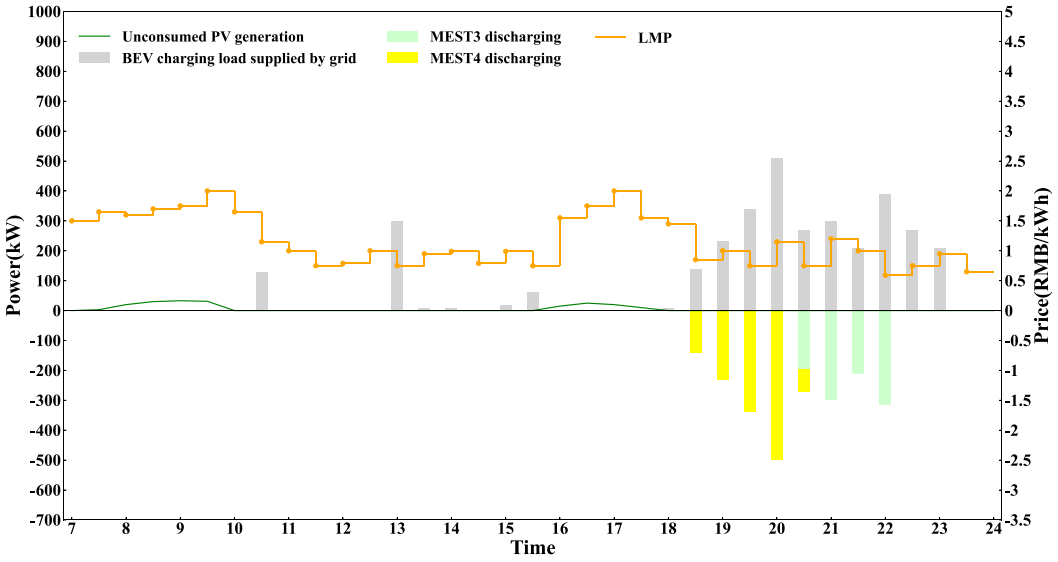


**Fig. 21.** MEST charging and discharging power, LMP, and unconsumed PV generation profiles in ESA5.

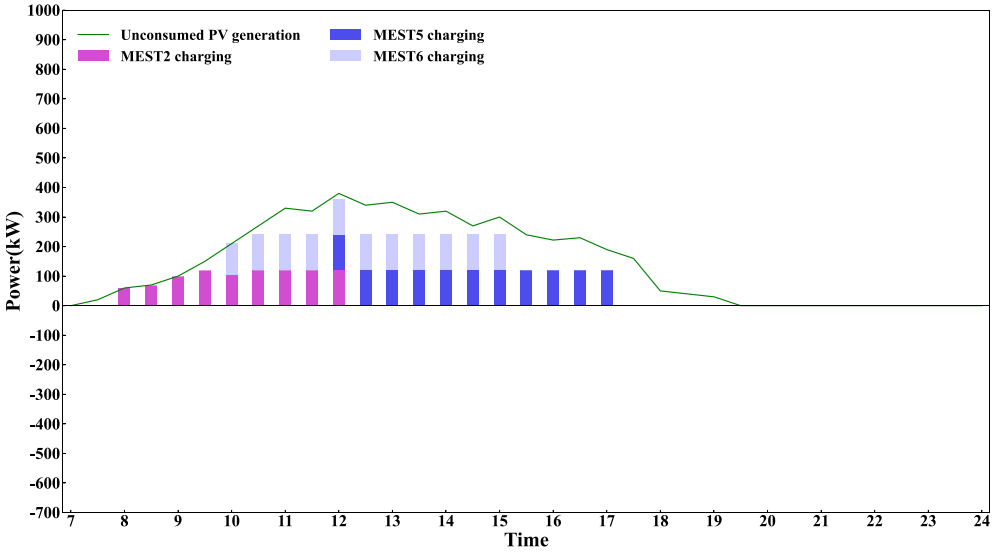


**Fig. 22.** MEST charging and discharging power, LMP, and unconsumed PV generation profiles at SPESP.

compared to the basic case, doubling the charging load limit. Every ESA has an installed PV capacity of 1.2 MW. Fig. 25 shows PV generation profiles in each time slot in seven ESAs and at the SPESP. PV generation in the extended case is approximately twice as much as in the basic case. The proposed first-stage method, based on the C&CG algorithm, converges after 11 iterations in the extended case, as shown in Fig. 26. The computational time in the extended case is approximately 360 min, which is acceptable for the day-ahead schedule.

Then, in the extended case, the PV generation utilization of the proposed two-stage approach, which incorporates MESTs, is compared with that of the first-stage method that excludes MEST scheduling. As shown in Fig. 27, the two-stage method achieves a 17.3% improvement in total PV generation utilization, highlighting the effectiveness of integrating MESTs into the scheduling process. This improvement is attributed to the MESTs' ability to transport excess PV generation (unutilized during BEV charging) in ESAs 1–2 and at the SPESP to locations with higher energy demands.

### 5.6. Sensitivity analysis

This section analyzes the sensitivity of the model employed in this study. Table 8 presents the variations in PV generation utilization and grid electricity purchase costs under different PV generation scenarios. The PV generation utilizations for both the proposed two-stage scheduling approach, which integrates MESTs, and the first-stage approach, which excludes MEST scheduling, are presented. The PV generation profiles for the basic case are illustrated in Fig. 6. In the PV-double case, the PV generation at the SPESP and in all ESAs is twice that of the basic case, while in the PV-triple case, it is three times higher across all time slots. All other parameters in the PV-double and PV-triple cases remain consistent with those in the basic case, as described in Section 5.1.

The results indicate that in both the PV-double and PV-triple scenarios, the PV generation utilization for the two-stage scheduling method is significantly greater than that of the first-stage method, underscoring the effectiveness of integrating MESTs into the scheduling process. For

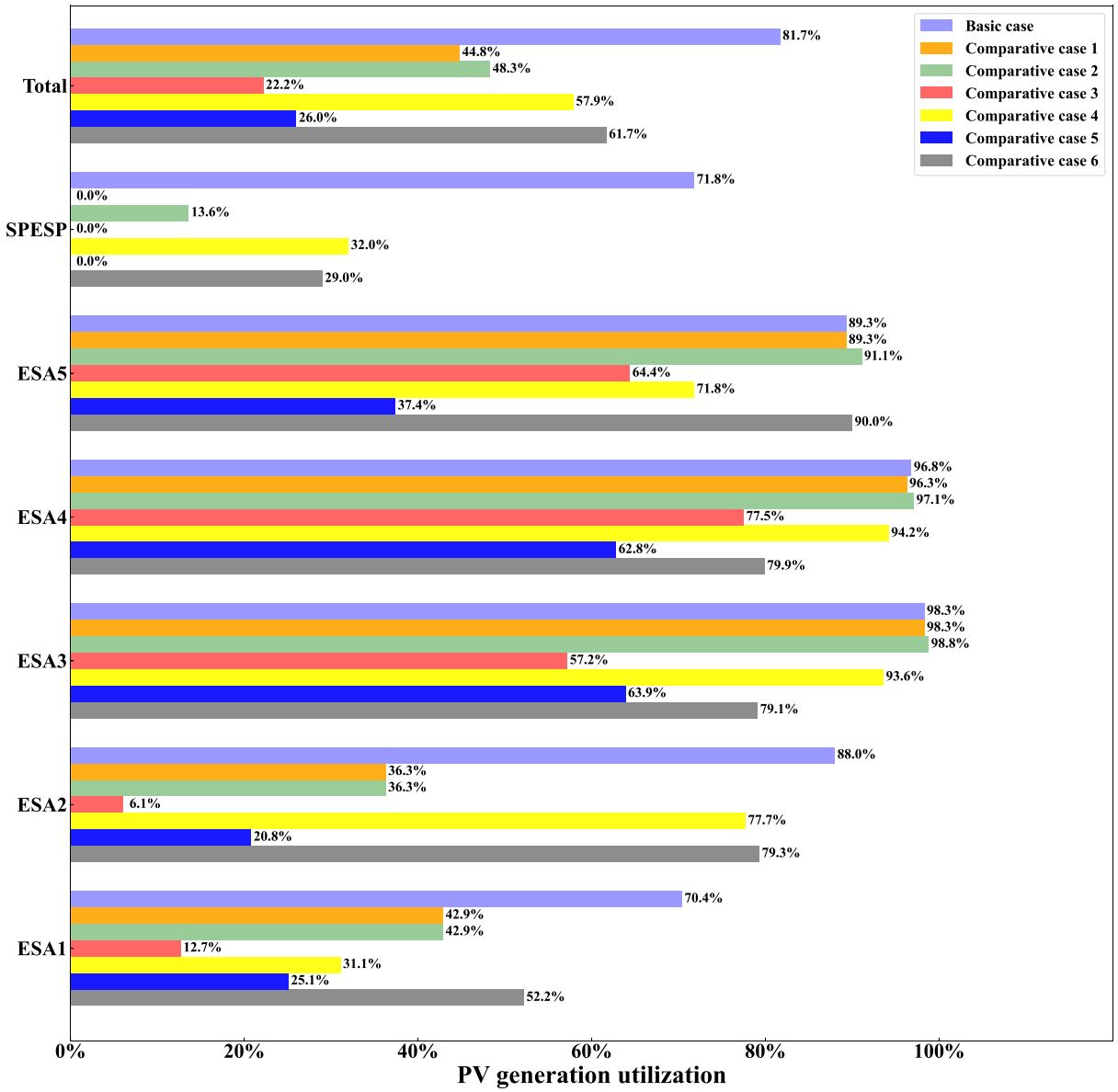


**Fig. 23.** PV generation utilization in comparative cases 1–6 and basic case.

instance, in the PV-double scenario, the utilization rate of PV generation under the two-stage scheduling method is 19.9% higher than that of the first-stage method. Furthermore, as PV generation increases exponentially, both PV generation utilization and grid purchase costs are substantially reduced. Specifically, under the two-stage scheduling method, the PV-double scenario results in a 31.2% reduction in PV generation utilization compared to the basic case, whereas the PV-triple scenario yields an additional 16.1% reduction relative to the PV-double case. Additionally, the PV-double scenario decreases the grid electricity purchase cost by 1429.1 RMB compared to the basic case.

The primary reason for these outcomes is that, with a fixed number of BEVs, their charging demand is limited, which constrains the ability to absorb higher levels of PV generation. This finding suggests that when investing in PV infrastructure, expressway managers should carefully consider BEV traffic flow to avoid overbuilding PV capacity that may not be fully utilized.

Table 9 shows the variations in PV generation utilization and grid purchase costs under different BEV number scenarios. The BEV number profiles for the basic case are illustrated in Figs. 7–8. In the BEV-double case, the number of BEVs entering the expressways at the Xi'an and Mianchi Entrances is twice that of in the basic case during each time slot. In contrast, the BEV-triple scenario sees this number tripled. All other parameters in the BEV-double and BEV-triple cases remain consistent with those in the basic case, as detailed in Section 5.1.

The results indicate that in both the BEV-double and BEV-triple cases, the PV generation utilization for the two-stage scheduling method is significantly higher than that of the first-stage method, demonstrating the effectiveness of integrating MESTs into the scheduling process. For instance, in the BEV-double case, PV generation utilization for the two-stage scheduling method is 30.5% higher than that of the first-stage method. As the number of BEVs on the expressways increases exponentially, PV generation utilization also rises. Under the first-stage method, the BEV-double case results in a 13.3% increase in PV generation utilization compared to the basic case, while the BEV-triple case further enhances PV generation utilization by 6.8% compared to the BEV-double case. This improvement is attributable to

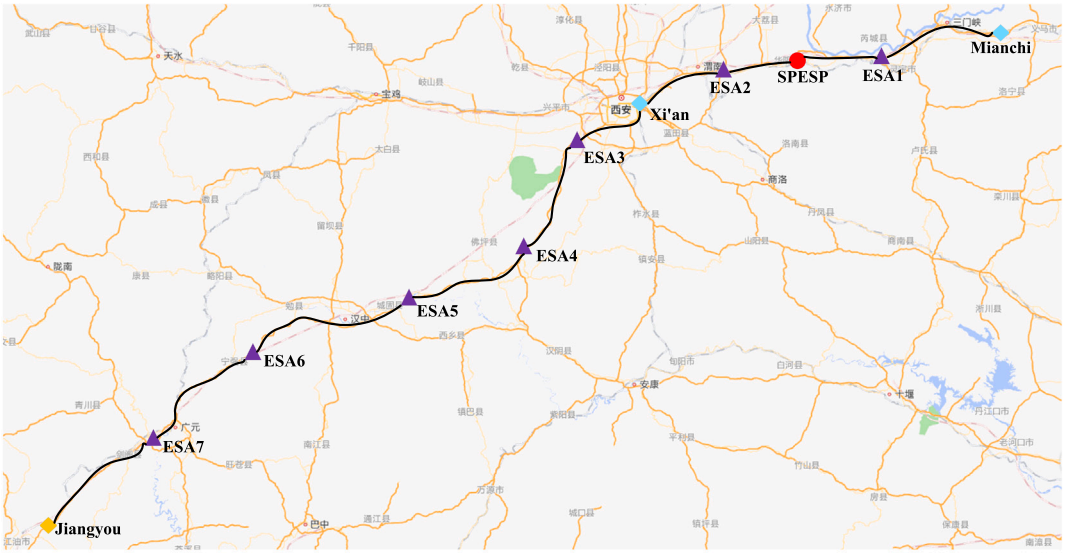


**Fig. 24.** Illustration of the expressway system in the extended case.

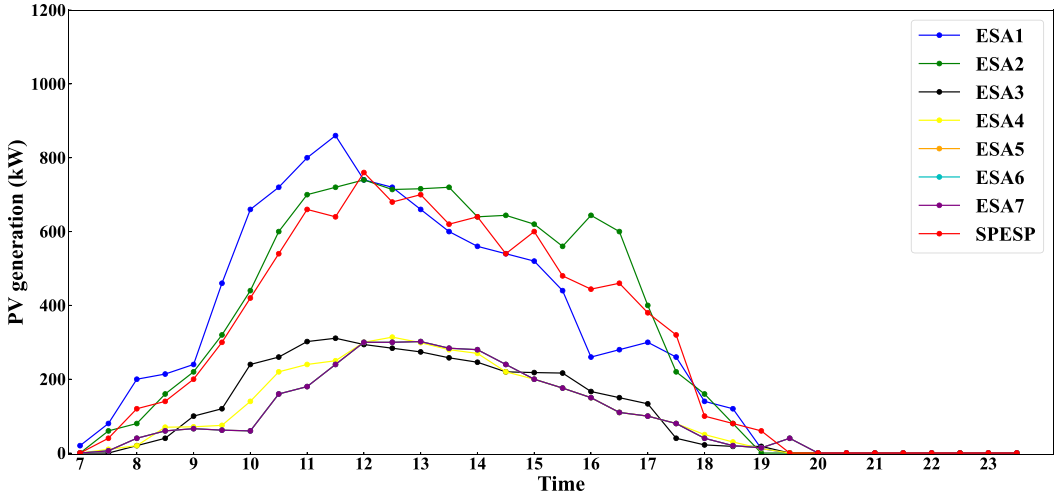


**Fig. 25.** PV generation along expressways in the extended case.

**Table 8**
Results of PV generation utilization and grid electricity purchase costs under different PV generation scenarios.

| Case | PV generation utilization | | Grid electricity purchase costs |
|---|---|---|---|
| | First-stage method (without MEST scheduling) | Two-stage method (with MEST scheduling) | |
| Basic case | 44.8% | 81.7% | 2122.0 RMB |
| PV-double case | 30.6% | 50.5% | 692.9 RMB |
| PV-triple case | 22.5% | 34.4% | 251.9 RMB |

**Table 9**
Results of PV generation utilization and grid electricity purchase costs under different number of BEVs scenarios.

| Case | PV generation utilization | | Grid electricity purchase costs |
|---|---|---|---|
| | First-stage method (without MEST scheduling) | Two-stage method (with MEST scheduling) | |
| Basic case | 44.8% | 81.7% | 2122.0 RMB |
| BEV-double case | 58.1% | 88.6% | 10365.2 RMB |
| BEV-triple case | 64.9% | 90.2% | 19168.0 RMB |

the increased charging demands of a higher number of BEVs, which allows for greater absorption of PV generation.

However, it is important to note that as the number of BEVs grows exponentially, the cost of purchasing electricity from the grid also rises significantly. For example, the BEV-double case incurs additional grid electricity purchase cost of 8243.2 RMB compared to the basic case, whereas the BEV-triple case raises this cost by an additional 8802.8 RMB relative to the BEV-double case. Given that PV generation along

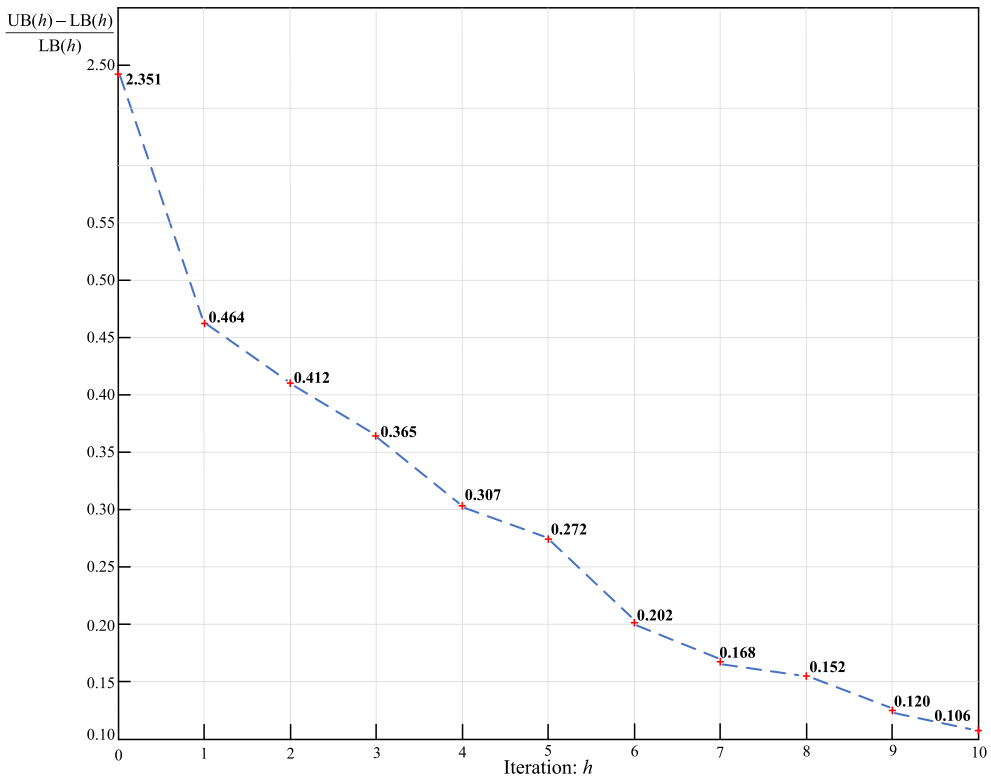


**Fig. 26.** Convergence of the proposed first-stage method in the extended case.

**Table 10**
Results of PV generation utilization and grid electricity purchase costs under different MEST operational parameter scenarios.

| Case | MEST operational parameters | | PV generation utilization (Two-stage method) | Grid electricity purchase costs |
|---|---|---|---|---|
| | $\upsilon^{ech}, \upsilon^{edis}$ | $\upsilon^{ep}$ | | |
| Basic case | 0.21 RMB/kWh | 3 RMB | 81.7% | 2122.0 RMB |
| MEST-double case | 0.42 RMB/kWh | 9 RMB | 65.1% | 3310.3 RMB |
| MEST-triple case | 0.63 RMB/kWh | 12 RMB | 52.2% | 4765.1 RMB |

the expressways remains unchanged in both the BEV-double and BEV-triple scenarios, the limited PV generation is insufficient to meet the exponentially growing BEV charging demands. Consequently, more electricity must be sourced from the grid to satisfy these charging loads. This finding underscores the critical importance of aligning BEV charging demand with the capacity of the PV system to ensure operational efficiency and minimize reliance on grid electricity.

Table 10 presents the variations in PV generation utilization and grid purchase costs across different scenarios involving MEST operational parameters. The scheduling costs for MEST arise from charging/discharging degradation expenses of the BESD ($\upsilon^{ech}, \upsilon^{edis}$) and the moving expenses per ES ($\upsilon^{ep}$). These parameters ($\upsilon^{ech}$, $\upsilon^{edis}$, and $\upsilon^{ep}$) are considered as operational parameters for MEST scheduling. In the MEST-double case, these operational parameters are doubled compared to the basic case for every time slot, while in the MEST-triple case, they are tripled.

The operational parameters only affect the second-stage scheduling model. The PV generation utilization for the first-stage method remains unchanged at 44.8% in both the MEST-double and MEST-triple cases, consistent with the basic case. As $\upsilon^{ech}, \upsilon^{edis}$, and $\upsilon^{ep}$ increase, the effectiveness of MEST scheduling in improving PV generation utilization diminishes significantly. Specifically, in the MEST-double case, scheduling MESTs results in a 20.3% increase in PV generation utilization, while in the MEST-triple case, the increase is even smaller—only 7.4%. Furthermore, as the operational parameters increase, the cost of purchasing electricity from the grid also rises. For example, the MEST-double case increases the grid electricity purchase cost by 1188.3 RMB compared to the basic case, while the MEST-triple case further raises the cost by an additional 1454.8 RMB compared to the MEST-double case.

These results suggest that as MEST operational parameters increase, the costs associated with using MESTs to provide clean energy for BEV charging become significantly higher. Consequently, it may become more cost-effective to rely on grid electricity to meet BEV charging demands rather than using MESTs. In the future, advancements in energy storage and transportation technologies are expected to reduce the operating costs of MEST scheduling, playing a crucial role in promoting green transportation.

## 6. Conclusion

This study proposes a two-stage scheduling approach for efficient PV generation resource allocation, considering the coupling relationship between BEV charging and MEST scheduling on expressways. This study aims to find the optimal management strategy for expressway PV generation resources by considering the perspectives of both drivers and the expressway manager. A spatial–temporal network model is developed to depict energy transfer from electricity supply to demand and geographical variations in traffic volume. The optimization problem is divided into two stages based on PV generation along expressways. The first-stage problem involves a two-layer optimization model to

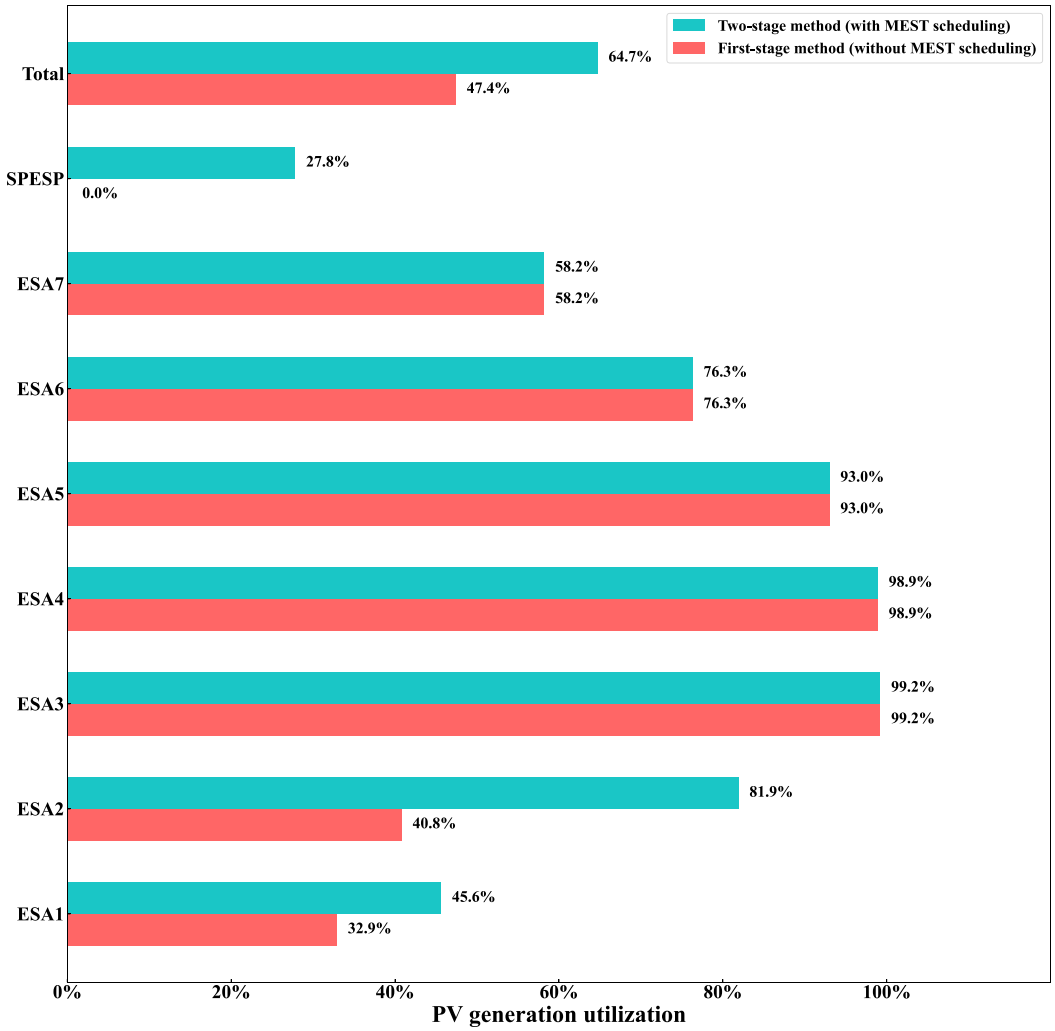


**Fig. 27.** Comparison of PV generation utilization with&without MEST scheduling in the extended case.

determine BEV charging schemes and balance the benefits between the expressway manager and BEV drivers. In detail, the upper-layer model maximizes the expressway manager's net earnings, whereas the lower-layer model minimizes the charging and parking expenses for BEV drivers. Meanwhile, the C&CG algorithm is utilized in the first stage to calculate PV generation unconsumed by BEV charging and grid-supplying charging loads in ESAs. The second stage introduces the MILP model to efficiently address the MEST scheduling problem and optimizes the allocation of unconsumed PV generation identified in the first stage.

Additionally, the proposed two-stage scheduling approach is validated by an expressway system with five ESAs, two entrances, one SPESP, and approximately 330 BEVs. The results of the first-stage problem reveal the challenge of addressing spatial supply–demand imbalances solely through reshaping BEV charging loads. In particular, the SPESP without charging demand provides PV generation of 2481 kWh, whereas ESA3 with PV generation of 987 kWh has charging demands of 3120 kWh. Moreover, the proposed method has the highest total PV generation utilization (81.7%) compared to six comparative cases. Particularly noteworthy is the 59.5% increase compared to the comparative case 3, highlighting the advantages of optimizing the coupled relationship between BEV charging and MEST scheduling. This finding suggests that the proposed MEST scheduling strategy, based on an energy supply–demand framework, significantly enhances PV generation utilization compared to approaches without considering PV generation and BEV charging loads. The electricity purchasing expense (roughly 2122 RMB) under the proposed method is the lowest compared to six comparative cases. In summary, the results indicate that the proposed two-stage scheduling approach can effectively schedule both BEV charging and MESTs to consume PV generation while achieving a win-win situation for both the economy and the environment of the expressway manager. Furthermore, the insights from this study extend beyond operational optimization, offering valuable implications for expressway infrastructure managers and policymakers. The two-stage scheduling approach shows how to make the most of solar power generation. It offers a useful way to connect building infrastructure with sustainability goals. This research highlights the need to include renewable energy in expressways to support policies for changing energy sources and protecting the environment.

Despite these advancements, this study still has several potential limitations. This study assumes uniform charging behavior for BEV users. However, real-world scenarios involve diverse charging patterns influenced by individual preferences, travel schedules, and other stochastic factors. These variations could significantly impact charging load distributions and the effectiveness of the proposed solution. Future research should incorporate models that account for heterogeneous user behavior, such as preference-based simulations or probabilistic demand models. Furthermore, this study focuses solely on the operational costs of MESTs related to the charging/discharging degradation of BESDs and vehicle movement. Other cost factors, such as maintenance and deployment, are not discussed in detail. While MESTs offer significant flexibility, challenges like high maintenance expenses, complex

deployment logistics, and regulatory constraints may create substantial barriers to real-world implementation. Future research should conduct comprehensive cost analysis to evaluate the life-cycle economic feasibility of MESTs and explore optimized strategies for maintenance and deployment to enhance their practicality and efficiency. Moreover, the proposed model is tailored for a specific expressway setup with particular traffic patterns and regulatory conditions. This may limit its applicability to other regions with different conditions. Future studies should evaluate the model's performance in diverse scenarios, such as varying traffic conditions or management patterns. Finally, this study focuses solely on utilizing renewable energy from PV systems. However, different regions may have access to other renewable energy sources along expressways, such as wind energy in coastal areas. Future research will explore the integration of these alternative renewable sources, leveraging their unique characteristics to enhance energy supply for BEV charging and further optimize the sustainability of expressway energy systems.

## CRediT authorship contribution statement

**Dawei Wang:** Writing – original draft, Methodology, Formal analysis, Conceptualization. **Jingwei Guo:** Writing – review & editing, Writing – original draft, Supervision, Methodology, Conceptualization. **Yongxiang Zhang:** Writing – review & editing, Methodology, Formal analysis, Conceptualization. **Qingwei Zhong:** Resources, Investigation, Data curation. **Hongke Xu:** Validation, Resources, Investigation.

## Declaration of competing interest

The authors declare that they have no known competing financial interests or personal relationships that could have appeared to influence the work reported in this paper.

## Acknowledgment

This work was supported by the National Key Research and Development Program of China under Grant (2021YFB2601401), the National Natural Science Foundation of China (No.72201218), and the Sichuan Science and Technology Program (2023NSFSC0901).

## Data availability

Data will be made available on request.

## References

[1] Hammam AH, Nayel MA, Mohamed MA. Optimal design of sizing and allocations for highway electric vehicle charging stations based on a PV system. Appl Energy 2024;376:124284. http://dx.doi.org/10.1016/j.apenergy.2024.124284.

[2] Yu J, Lu J. Slope stability analysis of expressway subgrade with photovoltaic facilities. In: 8th international conference on hydraulic and civil engineering - deep space intelligent development and utilization forum. ICHCE, Xi'an, China: IEEE; 2022, p. 588–93.

[3] Wu Y, Wu C, Zhou J, Zhang B, Xu C, Yan Y, Liu F. A DEMATEL-TODIM based decision framework for PV power generation project in expressway service area under an intuitionistic fuzzy environment. J Clean Prod 2020;247:119099. http://dx.doi.org/10.1016/j.jclepro.2019.119099.

[4] Aghalari A, Salamah D, Kabli M, Marufuzzaman M. A two-stage stochastic location–routing problem for electric vehicles fast charging. Comput Oper Res 2023;158:106286. http://dx.doi.org/10.1016/j.cor.2023.106286.

[5] Chen S-Y, Zhang J-X, Ni Q-C, Skitmore M, Ballesteros-Perez P, Ke Y-J, Zuo J, Sun H-J. Data-driven platform framework for digital whole-process expressway construction management. Front Neurosci 2022;16. http://dx.doi.org/10.3389/fnins.2022.891772.

[6] Wang W, Li C, He Y, Bai H, Jia K, Kong Z. Enhancement of household photovoltaic consumption potential in village microgrid considering electric vehicles scheduling and energy storage system configuration. Energy 2024;311:133330. http://dx.doi.org/10.1016/j.energy.2024.133330.

[7] De Wolf D, Smeers Y. Comparison of battery electric vehicles and fuel cell vehicles. World Electr Veh J 2023;14(9):262. http://dx.doi.org/10.3390/wevj14090262.

[8] Li X, Wang R. Towards integrated thermal management systems in battery electric vehicles: A review. ETransportation 2025;24:100396. http://dx.doi.org/10.1016/j.etran.2025.100396.

[9] Yao Z, Ran L, Wang Z, Guo X. Integrated management of electric vehicle sharing system operations and internet of vehicles energy scheduling. Energy 2024;309:132498. http://dx.doi.org/10.1016/j.energy.2024.132498.

[10] Song J, Yang Y, Xu Q. Two-stage robust optimal scheduling method for virtual power plants considering the controllability of electric vehicles. Electr Power Syst Res 2023;225:109785. http://dx.doi.org/10.1016/j.epsr.2023.109785.

[11] Zhang Y, Tan W, Ding Z. Highway charging station operator pricing considering distributed renewable generation resources. In: 2022 IEEE/IAS 58th industrial and commercial power systems technical conference. I&CPS, 2022, p. 1–6.

[12] Ullah Z, Wang S, Wu G, Hasanien HM, Rehman AU, Turky RA, Elkadeem MR. Optimal scheduling and techno-economic analysis of electric vehicles by implementing solar-based grid-tied charging station. Energy 2023;267. http://dx.doi.org/10.1016/j.energy.2022.126560.

[13] Tian K, Zang Y, Wang J, Zhang X. Strategic investments in mobile and stationary energy storage for low-carbon power systems. J Energy Storage 2024;101:113937. http://dx.doi.org/10.1016/j.est.2024.113937.

[14] Kim S, Joo S-K. Spatiotemporal operation method for mobile virtual power line in power system with mobile energy storage systems. J Energy Storage 2025;108:115196. http://dx.doi.org/10.1016/j.est.2024.115196.

[15] Arena G, Chub A, Lukianov M, Strzelecki R, Vinnikov D, De Carne G. A comprehensive review on DC fast charging stations for electric vehicles: Standards, power conversion technologies, architectures, energy management, and cybersecurity. IEEE Open J Power Electron 2024;5:1573–611. http://dx.doi.org/10.1109/OJPEL.2024.3466936.

[16] Baidu. Hubei blizzard in 2024. 2024, https://baike.baidu.com.

[17] Kim J, Dvorkin Y. Enhancing distribution system resilience with mobile energy storage and microgrids. IEEE Trans Smart Grid 2019;10(5):4996–5006. http://dx.doi.org/10.1109/TSTE.2020.3001015.

[18] Lei S, Chen C, Zhou H, Hou Y. Routing and scheduling of mobile power sources for distribution system resilience enhancement. IEEE Trans Smart Grid 2019;10(5):5650–62. http://dx.doi.org/10.1109/TSG.2018.2889347.

[19] Yan X, He X. Optimal cooperative scheduling strategy of energy storage and electric vehicle based on residential building integrated photovoltaic. J Build Eng 2024;95:110082. http://dx.doi.org/10.1016/j.jobe.2024.110082.

[20] Gong C, Yao Z, Chen H, Huang D, Wang X, Wang Z, Shi S. An optimal coordinated planning strategy for distributed energy station based on characteristics of electric vehicle charging behavior under carbon trading mechanism. Int J Electr Power Energy Syst 2023;147:108884. http://dx.doi.org/10.1016/j.ijepes.2022.108884.

[21] Abuelrub A, Hamed F, Hedel J, Al-Masri HMK. Feasibility study for electric vehicle usage in a microgrid integrated with renewable energy. IEEE Trans Transp Electr 2023;9(3):4306–15. http://dx.doi.org/10.1109/TTE.2023.3243237.

[22] Secchi M, Barchi G, Macii D, Petri D. Smart electric vehicles charging with centralised vehicle-to-grid capability for net-load variance minimisation under increasing EV and PV penetration levels. Sustain Energy Grids 2023;35:101120. http://dx.doi.org/10.1016/j.segan.2023.101120.

[23] Bartolucci L, Cordiner S, Mulone V, Santarelli M, Ortenzi F, Pasquali M. PV assisted electric vehicle charging station considering the integration of stationary first- or second-life battery storage. J Clean Prod 2023;383:135426. http://dx.doi.org/10.1016/j.jclepro.2022.135426.

[24] Tostado-Véliz M, Kamel S, Hasanien HM, Arévalo P, Turky RA, Jurado F. A stochastic-interval model for optimal scheduling of PV-assisted multi-mode charging stations. Energy 2022;253:124219. http://dx.doi.org/10.1016/j.energy.2022.124219.

[25] Abdalla MAA, Min W, Haroun GAH, Elhindi M. Optimal energy scheduling strategy for smart charging of electric vehicles from grid-connected photovoltaic system. In: 2021 7th international conference on electrical, electronics and information engineering. ICEEIE, IEEE Indonesia Sect; Univ Negeri Malang; Inovasi Bernas; 2021, p. 37–42. http://dx.doi.org/10.1109/ICEEIE52663.2021.9616634.

[26] Wang J, Guo Q, Sun H. Planning approach for integrating charging stations and renewable energy sources in low-carbon logistics delivery. Appl Energy 2024;372:123792. http://dx.doi.org/10.1016/j.apenergy.2024.123792.

[27] Deshmukh SS, Pearce JM. Electric vehicle charging potential from retail parking lot solar photovoltaic awnings. Renew Energy 2021;169:608–17. http://dx.doi.org/10.1016/j.renene.2021.01.068.

[28] Aguirre I, Davila-Sacoto M, Gonzalez LG, Hernandez-Callejo L, Duque-Perez O, Luis Zorita-Lamadrid A, Espinoza JL. Charge management of electric vehicles from undesired dynamics in solar photovoltaic generation. Appl Sci 2022;12(12):6246. http://dx.doi.org/10.3390/app12126246.

[29] Chen X, Wang X, Lu Z, Huang J, Huang Y. Distributed energy trading for electric vehicle charging stations equipped with distributed PV considering transportation network. Energy Rep 2023;9(8):819–27. http://dx.doi.org/10.1016/j.egyr.2023.04.303.

[30] Chowdary A, Rao SS. Grid-connected photovoltaic-based microgrid as charging infrastructure for meeting electric vehicle load. Front Energy Res 2022;10. http://dx.doi.org/10.3389/fenrg.2022.961734.
[31] Liang F, Ni J, Yu Z, Zhang K, Zhao Q, Wang S. Fixed and mobile energy storage coordination optimization method for enhancing photovoltaic integration capacity considering voltage offset. Front Energy Res 2024;12:1351324. http://dx.doi.org/10.3389/fenrg.2024.1351324.
[32] Shi W, Liang H, Bittner M. Stochastic planning for power distribution system resilience enhancement against earthquakes considering mobile energy resources. IEEE Trans Sustain Energy 2024;15(1):414–28. http://dx.doi.org/10.1109/TSTE.2023.3296063.
[33] Habibi S, Effatnejad R, Hedayati M, Hajihosseini P. Stochastic energy management of a microgrid incorporating two-point estimation method, mobile storage, and fuzzy multi-objective enhanced grey wolf optimizer. Sci Rep 2024;14(1):1667. http://dx.doi.org/10.1038/s41598-024-51166-9.
[34] Meng H, Xu T, Li M, Wei W, Sun J, Li K, Huangfu X, Yu H. Mobile energy storage system scheduling at low voltage distribution system. In: 2023 IEEE power & energy society general meeting. PESGM, IEEE power and energy society general meeting PESGM, 2023, p. 1–5. http://dx.doi.org/10.1109/PESGM52003.2023.10253116.
[35] Ghasemi S, Moshtagh J. Distribution system restoration after extreme events considering distributed generators and static energy storage systems with mobile energy storage systems dispatch in transportation systems. Appl Energy 2022;310:118507. http://dx.doi.org/10.1016/j.apenergy.2021.118507.
[36] Mishra DK, Ghadi MJ, Li L, Zhang J, Hossain MJ. Active distribution system resilience quantification and enhancement through multi-microgrid and mobile energy storage. Appl Energy 2022;311:118665. http://dx.doi.org/10.1016/j.apenergy.2022.118665.
[37] Zhou W, Zhao P, Lu Y. Collaborative optimal configuration of a mobile energy storage system and a stationary energy storage system to cope with regional grid blackouts in extreme scenarios. Energies 2023;16(23):7903. http://dx.doi.org/10.3390/en16237903.
[38] Jeon S, Choi D-H. Joint optimization of volt/VAR control and mobile energy storage system scheduling in active power distribution networks under PV prediction uncertainty. Appl Energy 2022;310:118488. http://dx.doi.org/10.1016/j.apenergy.2021.118488.
[39] Wang Y, Qiu D, Strbac G. Multi-agent deep reinforcement learning for resilience-driven routing and scheduling of mobile energy storage systems. Appl Energy 2022;310:118575. http://dx.doi.org/10.1016/j.apenergy.2022.118575.
[40] Abdeltawab HH, Mohamed YA-RI. Mobile energy storage scheduling and operation in active distribution systems. IEEE Trans Ind Electron 2017;64(9):6828–40. http://dx.doi.org/10.1109/TIE.2017.2682779.
[41] Ahmed HM, Sindi HF, Azzouz MA, Awad AS. Stochastic multi-benefit planning of mobile energy storage in reconfigurable active distribution systems. Sustain Energy Grids Netw 2023;36:101190. http://dx.doi.org/10.1016/j.segan.2023.101190.
[42] Moura P, Sriram U, Mohammadi J. Sharing mobile and stationary energy storage resources in transactive energy communities. In: 14th IEEE madrid powerTech conference. IEEE POWERTECH, IEEE; Comillas Univ Pontificia; IEEE Power & Energy Soc; IBERDROLA; CEPSA; REPSOL; RTDS Technologies; EDP; POWERSYS Solut; AXPO; ENGIE; 2021, p. 1–6. http://dx.doi.org/10.1109/PowerTech46648.2021.9494999.
[43] Yao S, Wang P, Liu X, Zhang H, Zhao T. Rolling optimization of mobile energy storage fleets for resilient service restoration. IEEE Trans Smart Grid 2020;11(2):1030–43. http://dx.doi.org/10.1109/TSG.2019.2930012.
[44] Lin S, Lin J, Jing R, Ye X, Han H, Bian Y, You Q. Energy, environmental, economic, and social assessment of photovoltaic potential on expressway slopes: A case in Fujian province, China. Energy Rep 2024;12:4374–89. http://dx.doi.org/10.1016/j.egyr.2024.09.066.
[45] Liu G, Huo Z, Wan H, Zucaro A, Fiorentino G, Lu Y, Yang Q. Evaluation of carbon sink and photovoltaic system carbon reduction along roadside space. J Clean Prod 2024;477:143812. http://dx.doi.org/10.1016/j.jclepro.2024.143812.
[46] Wang Y, Ye H. Nearly 90% of expressway service areas have built electric vehicle charging facilities. Technical report, Xinhua Daily Telegraph; 2023, http://dx.doi.org/10.28870/n.cnki.nxhmr.2023.004520.
[47] Gueller N, Martinelli R, Fanzeres B, Louzada D. Optimization of battery swapping stations with heterogeneity, charging degradation and PV-option. J Energy Storage 2023;74:109509. http://dx.doi.org/10.1016/j.est.2023.109509.
[48] Garcia MHC, Molina-Galan A, Boban M, Gozalvez J, Coll-Perales B, Sahin T, Kousaridas A. A tutorial on 5G NR V2X communications. IEEE Commun Surv Tutor 2021;23(3):1972–2026. http://dx.doi.org/10.1109/COMST.2021.3057017.
[49] Afshar S, Macedo P, Mohamed F, Disfani V. Mobile charging stations for electric vehicles — A review. Renew Sustain Energy Rev 2021;152:111654. http://dx.doi.org/10.1016/j.rser.2021.111654.
[50] Holt SB, Vinopal K. Examining inequality in the time cost of waiting. Nat Hum Behav 2023;7(4):545–55. http://dx.doi.org/10.1038/s41562-023-01524-w.
[51] Li Y, Li X, Zhang C, Wu T. Decomposition algorithms for the robust unidirectional quay crane scheduling problems. Comput Oper Res 2024;167:106670. http://dx.doi.org/10.1016/j.cor.2024.106670.
[52] Himmich I, Er Raqabi EM, El Hachemi N, El Hallaoui I, Metrane A, Soumis F. MPILS: An automatic tuner for MILP solvers. Comput Oper Res 2023;159:106344. http://dx.doi.org/10.1016/j.cor.2023.106344.
[53] AMAP. AMAP in China. 2025, https://www.amap.com/.
[54] Niu M-B, Wang H-C, Li J, Liu H, Yin R. Coordinated energy dispatch of highway microgrids with mobile storage system based on DMPC optimization. Electr Power Syst Res 2023;217:109119. http://dx.doi.org/10.1016/j.epsr.2023.109119.
[55] Ding Y, Qu G, Chen X, Wang J, Song J, He G. Deep reinforcement learning-based spatiotemporal decision of utility-scale highway portable energy storage systems. IEEE Trans Ind Appl 2023;1–10. http://dx.doi.org/10.1109/TIA.2023.3274729.
[56] BYD. Configuration table of 2025 han EV models. 2025, https://www.byd.com/cn/parameter-comparison.
[57] National Bureau of Statistics. China statistical yearbook -2022. 2022, https://www.stats.gov.cn.
[58] Zhou X, Lv M, Ji Y, Zhang S, Liu Y. Pricing curb parking: Differentiated parking fees or cash rewards? Transp Policy 2023;142:46–58. http://dx.doi.org/10.1016/j.tranpol.2023.08.005.
[59] Azad-Farsani E, Abedini S, Sardou IG. Optimal coordination of plug-in hybrid electric vehicles: A stochastic market-based approach. J Clean Prod 2021;321:128990. http://dx.doi.org/10.1016/j.jclepro.2021.128990.
[60] Luo L, He P, Gu W, Sheng W, Liu K, Bai M. Temporal-spatial scheduling of electric vehicles in AC/DC distribution networks. Energy 2022;255:124512. http://dx.doi.org/10.1016/j.energy.2022.124512.
[61] Ministry of Ecology and Environment of China. Calculation of carbon emission factors for electricity. 2024, https://www.mee.gov.cn/.